Artificial selection of microbial communities can become effective after using evolution-informed strategies

Li Xie* , Alex Yuan, and Wenying Shou*

*Basic Sciences Division, Fred Hutchinson Cancer Research Center, Seattle, WA, 98102

Abstract

Multi-species microbial communities often display "community functions" stemming from interactions of member species. Interactions are often difficult to decipher, making it challenging to design communities with desired functions. Alternatively, similar to artificial selection for individuals in agriculture and industry, one could repeatedly choose communities with the highest functions to reproduce by randomly partitioning each into multiple "Newborn" communities for the next cycle. However, community selection is challenging since rapid changes in species and genotype compositions can limit the heritability of community function. To understand how to enact community selection, we used an individual-based model to simulate this process to improve a community function that requires two species and is costly to one species. Improvement was stalled by non-heritable variations in community function, such as the stochastic populating of Newborn communities or measurement errors of community function. Community function improved when these non-heritable variations were suppressed in experimentally feasible manners.

Introduction

Multi-species microbial communities often display important *functions*, defined as biochemical activities not achievable by member species in isolation. For example, a six-species microbial community, but not any member species alone, cleared relapsing *Clostridium difficile* infections in mice [1]. Community functions arise from *interactions* where an individual alters the physiology of another individual. Thus, to improve community function, one could identify and modify interactions [2, 3]. In reality, this is no trivial task: each species can release tens or more compounds, many of which may influence the partner species in diverse fashions [4, 5, 6, 7]. From this myriad of interactions, one would then need to identify those critical for community function, and modify them by altering species genotypes or the abiotic environment. One could also artificially assemble different combinations of species or genotypes at various ratios to screen for high community function. However, the number of combinations becomes very large even for a moderate number of species and genotypes.

*Author of correspondence

In an alternative approach, artificial selection of whole communities could be carried out over cycles to improve community function [8, 9, 10, 11, 12] (reviewed in [13, 14, 15]). A selection cycle starts with a collection of low-density communities with artificially-imposed boundaries (e.g. inside culture tubes). These low-density communities are incubated for a period of time during which community members multiply and interact with each other and possibly mutate, and the community function of interest (e.g. pollutant degradation) develops. At the end of incubation, desired communities (e.g. those degrading the most pollutant) are chosen to "reproduce" where each is randomly partitioned into multiple low-density communities to start the next cycle. Superficially, this process may seem straightforward since "one gets what one selects for". After all, artificial selection on individuals has been successfully implemented to obtain, for example, proteins of enhanced activities (Figure S1). However, compared to artificial selection of individuals or mono-species groups, artificial selection of multi-species communities is more challenging due to the limited heritability of community function. This is because community function, determined by species and genotype compositions, can change rapidly from one selection cycle to the next due to ecology and evolution (see detailed explanation in Figure S1). For example, member species critical for community function may get lost during growth and selection cycles. Consequently, artificial selection on whole communities has rarely been attempted.

The few attempts of community selection have generated interesting results. One theoretical study simulated artificial selection on multi-species communities based on their ability to modify their abiotic environment [10]. Communities responded to selection, but the response quickly leveled off, and could be generated without mutations. Thus, in this case, selection acted on species types instead of new genotypes [10]. In experiments, complex microbial communities were selected to improve their abilities to degrade a pollutant or to alter plant physiology [8, 9, 12, 11]. For example, microbial communities selected to promote early or late flowering in plants were dominated by distinct species types [11]. Interestingly in other cases, a community trait may fail to improve despite selection, and may improve even without selection [8, 9].

Intriguing as these selection attempts might be, much remains unknown. First, was the trait under selection a community function or an attribute of a single species? If the latter, then community selection may not even be needed. Second, did selection act solely on species types or also on newly-arising genotypes? If the former ([10, 11]), then without immigration of new species, community function may quickly level off [10]. If the latter, then community function could continue to improve as new genotypes evolve. Finally, why might a community trait sometimes fail to improve despite selection [8, 9]?

We are particularly interested in using artificial community selection to improve "costly" community functions. A community function is costly if any community member's fitness is reduced by contributing to that community function. Costly community functions are common in engineered microbial communities [16]. To improve a costly community function, artificial community selection must overcome natural selection which favors low community function.

To understand how to effectively enact community selection to improve a costly community function, here we simulate artificial selection of communities consisting of two defined species. Since a two-species community is simpler than most natural communities, we can mechanistically investigate how community members evolve under community selection. We also designed our simulations to mimic real lab experiments so that our conclusions can guide future experiments. For example, model parameters, including species phenotypes, mutation rate, and distribution of mutation effects, are based on a wide variety of published experiments. Thus, our model differs from previous models which focused on binary phenotypes (e.g. contributing or not contributing to community function) [17]. In addition, our model incorporates chemical mechanisms of species interactions, as advocated by [18, 19]. Our simulations show that artificial community selection can work with as few as 100 communities. However, this requires suppression of non-heritable variations in community function, including those caused by

routine experimental procedures such as pipetting and those caused by measurement errors of community function.

Results

We will first introduce the target of our community selection simulation: a two-species community that converts substrates to a valued product. We will then demonstrate conditions for species coexistence, define community function, and describe how we simulate community dynamics and artificial community selection. Finally, from simulation results, we will discuss how to make artificial community selection effective. To avoid confusion, we will use "community selection" or "selection" to describe the entire process of artificial community selection (community formation, growth, selection, and reproduction), and use "choose" to refer to the selection step.

A Helper-Manufacturer community that converts substrates into a product

Motivated by previous successes in engineering two-species microbial communities that convert substrates into useful products [20, 21, 22], we numerically simulated selection of such communities. In our community (Figure 1), Manufacturer M can manufacture Product P of value to us (e.g. a bio-fuel or a drug), but only if helped by Helper H. Specifically, Helper but not Manufacturer can digest an agricultural waste (e.g. cellulose), and as Helper grows, it releases Byproduct B at no fitness cost to itself. Manufacturer requires H's Byproduct (e.g. carbon source) to grow. In addition, Manufacturer invests f_P ($0 \leq f_P \leq 1$) fraction of its potential growth to make Product P while using the rest (1-f_P) for its biomass growth. Both species also require a shared Resource R (e.g. nitrogen). Thus, the two species together, but not any species alone, could convert substrates (Waste and Resource) into Product.

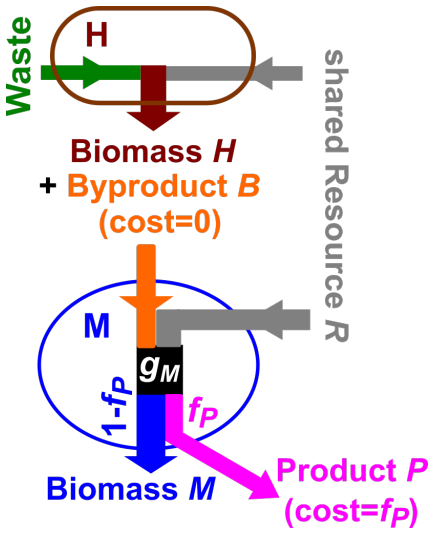

Figure 1: **A Helper-Manufacturer community that converts substrates into a product.** Helper H consumes Waste (present in excess) and Resource to grow biomass, and concomitantly releases Byproduct B at no fitness cost to itself. H's Byproduct B is required by Manufacturer M. M consumes Resource and H's Byproduct, and invests a fraction f_P of its potential growth g_M to make Product P while channeling the remaining to biomass growth. When biomass growth ceases, Byproduct and Product will no longer be made. The five state variables (italicized) H, M, R, B, and P correspond to the amount of H biomass, M biomass, Resource, Byproduct, and Product in a community, respectively.

Helpers and Manufacturers can coexist only under certain conditions

During each community selection cycle, we assemble low-density "Newborn" H-M communities and supply each with a fixed amount of Resource. We will then allow these Newborn communities to grow ("mature") over a fixed time T into high-density "Adult" communities during which community function develops. To achieve high community function, we want H and M species to coexist throughout community maturation. Furthermore, species ratio should not be extreme, because otherwise the low-abundance species could be lost by chance during community formation.

To achieve these goals, we note that upon Newborn formation, H can immediately start to grow on Waste and Resource. In contrast, M cannot grow until H's Byproduct has accumulated. Thus, if M always grows slower than H, the community would devolve to a single species H. Consequently, sustained coexistence requires that M's growth rate exceeds H's growth rate at some point during community maturation. We thus assigned the maximal birth rate achievable by M in excess nutrients to exceed that achievable by H (Table 1, Methods Section 2). A related requirement for coexistence is that the fraction growth M diverts for making Product (f_P) must not be too large, or else M would always grow slower than H and thus go extinct (Figure 2 top).

In the H-M community, the steady state species ratio is a function of f_P as well as c_{BM} - the amount of Byproduct consumed per M biomass grown divided by the amount of Byproduct released per H biomass grown (Eq. 14 in Methods; Table 1). To achieve moderate specie ratio, $1 - f_P$ and c_{BM} need to be of comparable magnitude. We chose parameters so that different initial species ratios would converge to a moderate steady state value (Figure 2, bottom). All our parameters were based on

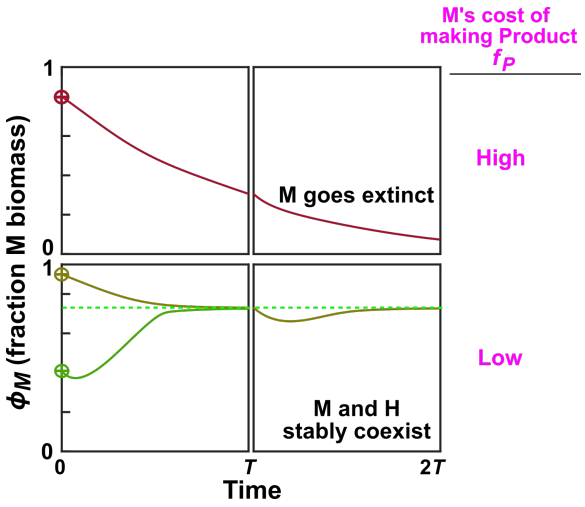

Figure 2: **H and M can stably coexist at low** f_P. Here, we plotted the fraction of M biomass of a community over two maturation cycles. **Top**: When f_P**,** the fraction of potential growth Manufacturer diverts for making Product, is high (e.g. $f_P = 0.8$), M goes extinct. **Bottom**: At low f_P (e.g. $f_P = 0.1$), H and M can stably coexist. That is, species ratio will converge to a steady state value. Calculations were based on equations 6-10 with parameters in the last column of Table 1. At the end of the first cycle (time T), Byproduct and Resource were re-set to the initial conditions at time zero, and total biomass was reduced to BM_{target} while ϕ_M remained the same as that of the parent community.

published yeast and *E. coli* measurements (Table 1, Methods Section 2). Note that species coexistence at a moderate ratio has been experimentally realized in engineered communities [20, 21, 23, 24].

Simulating community dynamics and selection

We define community function as the total amount of Product accumulated as a low-density Newborn community grows into an Adult community over maturation time T, i.e. $P(T)$ (Figure 3, top two rows). In Methods Section 7, we explain problems associated with alternative definitions of community function (e.g. per capita production). Community function is not costly to Helpers, but reduces M's growth rate by fraction f_P (Figure 1).

We simulate four stages of community selection (Figure 3): formation of Newborn communities; Newborn communities maturing into Adult communities; choosing highest-functioning Adult communities, and reproducing the chosen Adult communities by splitting each into multiple Newborn communities of the next cycle. Our simulation is individual-based, tracking phenotypes and biomass of individual H and M cells in each community as cells grew, divided, mutated, or died. Our simulations also tracked dynamics of chemicals (including Product) in each community, and described the actual experimental steps such as pipetting cultures during community reproduction. Below, we describe model structure, and parameters that we can vary for different community selection regimens.

Model structure

Our simulation started with n_{tot} number of Newborn communities (Methods Section 6). Each Newborn community always started with a fixed amount of Resource and a total biomass close to a target value BM_{target} (see Methods Section 7 for problems associated with not having a biomass target). Waste was

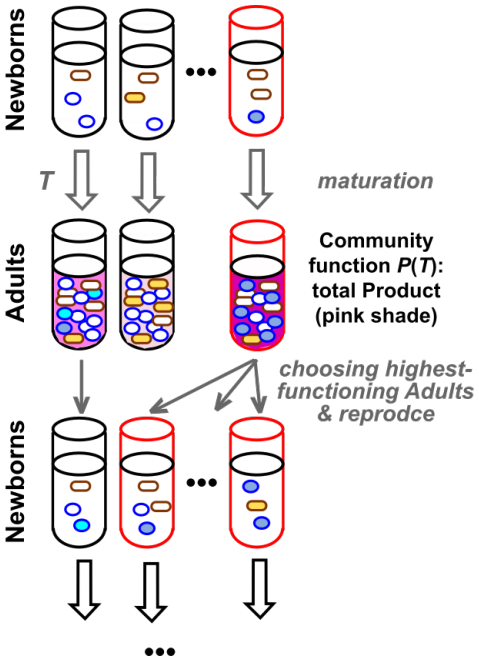

Figure 3: **Community selection scheme.** In our simulations, cycles of selection were performed on a total of $n_{tot} = 100$ communities. At the beginning of the first cycle, each Newborn had a total biomass of BM_{target}=100 (60 M and 40 H each of biomass 1). In subsequent cycles, species ratio would converge to the steady state value (Figure2 bottom). Waste (not drawn) was in excess. The amount of Resource in each Newborn (not drawn) was fixed at a value that could support a total biomass of 10^4. The maturation time T was chosen so that for an average community, Resource was not depleted (in experimental terms, this would avoid complications of the stationary phase). During maturation, Resource R, Byproduct B, Product P, and each cell's biomass were calculated from differential equations (Methods, Section 6). Death occurred stochastically to individual cells. A cell divided into two identical daughter cells once its biomass had reached a threshold of 2. After division, mutations (different shades of oval and rod) occurred stochastically to change a cell's phenotypes (maximal growth rate, affinity for metabolites, and M's f_P). At the end of a cycle (time T), the top-functioning Adult with the highest Product $P(T)$ was chosen and diluted into as many Newborns as possible so that on average, each Newborn had a total biomass of approximately BM_{target}. We then proceeded to the next top-functioning Adult until $n_{tot} = 100$ Newborns were generated for the next selection cycle. Communities with red outlines exemplify one lineage.

always supplied in excess and thus did not enter our equations. Note that except for the first cycle, the relative abundance of species in a Newborn community inherited that of the parent Adult community and remained at around the steady state value (Figure 2 bottom).

During community maturation, biomass of individual cells grew. The biomass growth rate of an H cell depended on Resource concentration (Monod Equation; Figure S4A; Eq. 23). As H grew, it consumed Resource and released Byproduct (Eqs. 21 and 22). The potential growth rate of an M cell depended on the concentrations of Resource and H's Byproduct ([25]; Figure S4B; see experimental support in Figure S5). M cell's actual biomass growth rate was$(1 - f_P)$ fraction of M's potential growth rate (Eq. 24). As M grew, it consumed Resource and Byproduct (Eqs. 21 and 22), and released Product at a rate proportional to f_P and M's potential growth rate (Eqs. 8). Meanwhile, cells died stochastically at a constant death rate. Once a cell's biomass grew from 1 to 2, it divided into two cells of equal biomass with identical phenotypes, thus capturing continuous biomass increase (Figure S3) as well as discrete cell division events observed experimentally [26]. Although mutations can occur during any stage of the cell cycle, we assigned mutations immediately after cell division, and each phenotype of each new cell mutated independently.

Mutable phenotypes included H and M's maximal growth rates and affinities for nutrients, and M's f_P (fraction potential growth diverted for making Product), since these phenotypes have been observed to rapidly change during evolution ([27, 28, 29, 30]). Mutated phenotypes could range between 0 and their respective upper bounds. On average, half of the mutations abolished the function (e.g. zero growth rate, zero affinity, or $f_P = 0$) based on experiments on GFP, viruses, and yeast [31, 32, 33]. Effects of the other 50% mutations were bilateral-exponentially distributed, enhancing or diminishing a phenotype by a few percent, based on our re-analysis of published yeast data sets [34] (Figure S8). We held release and consumption coefficients constant. This is because, for example, the amount of Byproduct released per H biomass generated is constrained by biochemical stoichiometry.

At the end of community maturation (time T), we obtained the community function $P(T)$ - the total amount of Product in the Adult community. After comparing community function of all Adults, we chose the highest-functioning Adult and split it randomly into Newborns of the target total biomass BM_{target}. For example, if the chosen Adult had a total biomass of $60BM_{target}$, then each cell would be assigned a random integer from 1 to 60, and those cells with the same random integer would be allocated to the same Newborn. Experimentally, this is equivalent to dilution by volume using a pipette. Thus, for each Newborn, the total biomass and species ratio fluctuated around their expected values in a fashion associated with pipetting. When the highest-functioning Adult was used up, the next highest-functioning Adult was chosen and reproduced until n_{tot} Newborns were generated for the next selection cycle.

Our model captures the alternating force of natural and artificial selection: Natural selection favors faster growers during community maturation, and artificial selection for high community function allows the highest-functioning communities to reproduce at the end of each selection cycle.

Parameters of selection regimen

Parameters of selection regimen include the total number of communities under selection (n_{tot}), Newborn target total biomass (BM_{target}), the amount of Resource added to each Newborn ($R(0)$), the amount of mutagenesis which controls the rate of phenotype-altering mutations (μ), and maturation time (T). To ensure successful community selection, these parameters must be carefully chosen.

If the total number of communities n_{tot} is very large, then the chosen community will likely display a higher community function than if n_{tot} is small, but the experimental setup is more challenging. We chose a total of 100 communities (n_{tot}=100).

If the mutation rate is very low, then community function cannot rapidly improve. If the mutation

rate is very high, then non-producers will be generated at a high rate and community function will be reduced. Here, we chose μ, the rate of phenotype-altering mutations, to be biologically realistic (0.002 per cell per generation per phenotype, which is lower than the highest values observed experimentally; Methods Section 4).

If Newborn total biomass BM_{target} is very large, or if the number of generations within T is very large, then non-producers will take over in all communities during maturation. This reduces the variance among Adults and limits the potential for selection (Figure S2, compare **A**-**C** with **D**). On the other hand, if both BM_{target} and the number of generations within T are very small, mutations will be rare within each cycle, and many cycles will be required to improve community function. Finally, if BM_{target} is very small, then a member species might get lost by chance during Newborn formation. In our simulations, we chose Newborn's target total biomass BM_{target}=100 biomass (e.g. 60 M cells and 40 H cells at 1 biomass/cell in the first cycle; cell biomass varying between 1 and 2 in later cycles). Unless otherwise stated, we fixed the input Resource $R(0)$ to support a maximal total biomass of 10^4, and chose maturation time T so that total biomass would undergo ~6 doublings (increasing to ~6400). Thus, by the end of T, $\leq$70% Resource would be consumed by an average community. This meant that when implemented experimentally, we could avoid complications associated with stationary phase while not wasting too much Resource.

Since T was relatively short (~6 doublings), new mutations arising during maturation would not have a chance to increase to a high enough frequency to impact community function. Thus in our selection regimens, community function would be largely determined by phenotypes of each H and M cells in the Newborn community, a point that would become important later.

Improved growth phenotypes can increase or decrease community function

In the absence of artificial selection for high community function, natural selection drove community function to zero as expected. Specifically, when Adult communities were randomly chosen to reproduce, community function consistently declined to zero (Figure S10C) as fast-growing non-producing M ($f_P = 0$) took over (average f_P declining to zero in Figure S10B).

During community selection, natural selection still operates throughout community maturation. Natural selection favors improved growth parameters, which can increase or decrease community function depending on, for example, the evolutionary bounds of species phenotypes. Suppose that g_{Hmax} and g_{Mmax}, H and M's maximal growth rates in excess nutrients, have evolutionary upper bounds g^*_{Hmax} and g^*_{Mmax}, respectively. If $g^*_{Hmax} > g^*_{Mmax}$, then community function could decline despite community selection (Figure4 A, left bar < 1). In this case, natural selection improved H's growth more than it improved M's growth, and consequently, communities became overwhelmingly dominated by H (Figure S13; n) and community function was low. Consistent with this observation, if growth parameters were not allowed to mutate, community function did not decline (Figure4 A, right bar being near 1). In contrast, if $g^*_{Hmax} < g^*_{Mmax}$, community function could improve more if growth parameters were allowed to improve compared to if growth parameters were fixed (Figure4 B). In this case, due to the lower evolutionary upper bound of g_{Hmax} compared to that of g_{Mmax}, H did not evolve to grow so fast to overwhelm M, and as natural selection improved H and M's growth parameters (Figure S12), faster growing H generated more Byproduct, resulting in larger M populations, higher Product level and community function. Thus, the evolutionary upper bounds of species phenotypes can affect the efficacy of community selection.

In all following simulations, we focused on scenarios where improving growth parameters of H and M generally improves community function (e.g. Figure4 B). This allows us to simplify the simulations

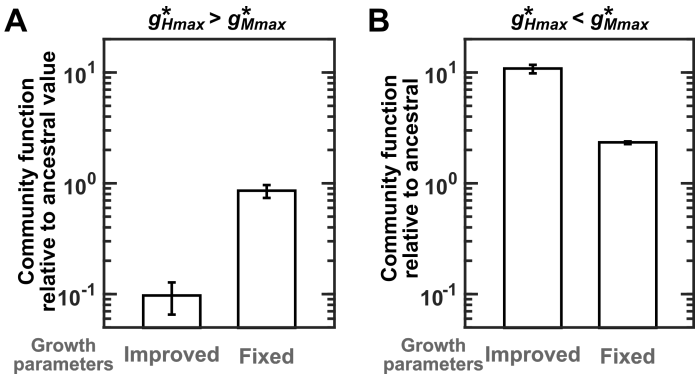

Figure 4: Improved growth parameters could (**A**) reduce community function or (**B**) improve community function depending on the evolutionary upper bounds of growth phenotypes. Each bar represents the selected community function after 1500 cycles divided by the community function of the ancestral community. Note the logarithmic scale of the y axis. (**A**) The evolutionary upper bound of the maximal growth rate of H exceeds that of M ($g^*_{Hmax} = 0.8 > g^*_{Mmax} = 0.7$). When H and M's growth parameters were allowed to mutate, community function was lower than if growth parameters were fixed to the ancestral values (the left bar being lower than the right bar). In these simulations, since H evolved to grow very fast, we adjusted initial Resource $R(0)$ to support 10^5 total biomass (higher than the standard 10^4 total biomass). (**B**) The evolutionary upper bound of the maximal growth rate of M exceeds that of H ($g^*_{Hmax} = 0.3 < g^*_{Mmax} = 0.7$, Table 1). When H and M's growth parameters were allowed to mutate, community function increased to a higher level compared to when growth parameters were fixed to the ancestral values (the left bar higher than the right bar). In these simulations, $R(0)$ supported standard amount (10^4) of total biomass. In both (**A**) and (**B**), natural selection improved growth parameters when growth parameters were allowed to mutate.

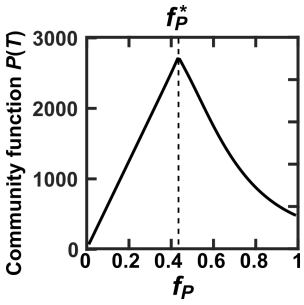

Figure 5: **An intermediate f_P is optimal for community function.** For a Newborn H-M community with a fixed total biomass $BM(0) = BM_{target} = 100$, supplied with a fixed Resource and excess Waste, and allowed to grow for maturation time $T = 17$ time units, maximal $P(T)$ is achieved at an intermediate $f_P^* = 0.41$ (dashed line). Here the Newborn community has 54 M and 46 H cells of biomass 1, which corresponds to the species composition optimal for $P(T)$ under these conditions. The corresponding maximal $P^*(T)$ could not be further improved if we allowed all growth parameters and f_P to mutate (Figure S20). Thus, $P^*(T)$ is locally maximal in the sense that small deviation will always reduce $P(T)$.

by fixing H and M's growth parameters to their upper bounds and only allowing f_P to mutate. This simplification is justified for three reasons. First, during these community selection simulations, growth parameters important to community function improved to their upper bounds (Figure S12C). Second, suppose that a mutation changes a growth parameter already at its upper bound. Since the growth parameter is already at its upper bound, the mutation can only reduce it, and thus, the mutant is disfavored by natural selection. And since we are studying cases where improving growth parameters improves community function, the mutant will also reduce community function and hence its host community is less likely to reproduce. Overall, the mutant will not persist which means that the growth parameter will remain at its upper bound. Third, our conclusions hold regardless of whether we fix growth parameters or not (Figure S15).

After fixing growth parameters, we can now focus on how f_P values of M cells evolve during community selection. f_P is of particular importance because engineered microbes pay a fitness cost to synthesize a product. An M cell with a higher f_P will grow slower than a low-producer, and thus be selected against by natural selection during community maturation. However, an M cell with higher f_P will result in higher community function, and thus its host community has a higher chance of being chosen to reproduce. As we will demonstrate, proper design of community selection regimen is critical to counter natural selection and successfully improve costly community function. Our conclusions hold even for the more difficult case of Figure4 A where improving growth parameters reduces community function (Figure S14).

Maximal community function is achieved at intermediate f_P

Once we had fixed all growth parameters to their respective upper bounds ("growth-adapted" H and M), we could calculate the f_P that would yield maximal community function. An intermediate f_P value ($f_P^* = 0.41$; Figure 5A) maximized community function. This is not surprising: at zero f_P, no Product would be made; at high f_P, M would go extinct (Figure 2 top panel).

Ineffective community selection is due to non-heritable variations in community function

We simulated community selection after fixing all growth parameters to evolutionary upper bounds and allowing only f_P to be modified by mutations. As described in "Model structure," we simulated community maturation by tracking the biomass growth of each H and M cells, cell division and death, mutation in f_P of each M cell, and metabolite release and consumption. We simulated community reproduction by incorporating stochastic fluctuations associated with volumetric dilution of the Adult community into Newborn communities using a pipette. Both f_P and community function $P(T)$ barely improved over thousands of selection cycles, even though both were far from their theoretical maxima (Figure 6A and B). Note that community function was above the ancestral value ((Figure 6B, brown star) because growth parameters were fixed to evolutionary upper bounds.

To understand why community selection failed to improve community function, we examine the heredity of the community function through identifying the determinants of the community function and examining whether these determinants are heritable. The community function of an H-M community is largely determined by phenotypes of each H and M cells in the Newborn community. This is because we had chosen a sufficiently short maturation time such that new genotypes arising during maturation could not rise to high frequency. The phenotypes of each H and M cells in the Newborn community can be approximated by the following three independent determinants of the community function: Newborn's total biomass $BM(0)$, Newborn's fraction of M biomass $\phi_M(0)$, and the average f_P over all M cells in Newborn $\overline{f}_P(0)$ (Eq 6-10). Note that because the composition of a community varies as it goes from its Newborn stage to its Adult stage, these determinants are all defined at a community's Newborn stage. A determinant is considered heritable if the determinant of a parent community (e.g. the red tube from the top row of Figure 3) and the determinants of its offspring communities (red tubes from the bottom row of Figure 3) are correlated. Among the three determinants, $\overline{f}_P(0)$ can be considered "heritable" as shown in Figure S29: if a parent community has a high $\overline{f}_P(0)$, i.e. a high average f_P at its Newborn stage, it will have a high average f_P at its Adult stage. Since its offspring communities inherit its M cells, they will have high $\overline{f}_P(0)$. On the other hand, Newborn total biomass $BM(0)$ is not heritable since it is not correlated between a parent community and its offspring communities, as shown in Figure S29. This is because when an Adult community reproduced, the dilution factor was adjusted so that the total biomass of an offspring Newborn community was on average the constant target biomass BM_{target}. The fraction of M biomass of a Newborn $\phi_M(0)$ is not heritable either, as shown in Figure S29. This is because although the fractions of M biomass of offspring Newborn communities are correlated with the fractions of M biomass of their parent community at Adult stage, the fractions of M biomass of a community at its Adult stage is not correlated with its fractions of M biomass at Newborn stage. As shown in the lower panel of Figure 2 between time 0 and T, different fractions of M biomass in the Newborn communities $\phi_M(0)$ approach a common steady-state value as they reach their Adult stages due to ecological interactions.

In successful community selection, higher community function should correlate with higher average Newborn f_P ($\overline{f}_P(0)$), because the latter is the heritable determinant of the former. However, we observed little correlation between community function $P(T)$ and $\overline{f}_P(0)$, but strong correlation between community function and its non-heritable determinants (Figure 7). For example, the Newborn that would achieve the highest function (left magenta dot) had a below-median $\overline{f}_P(0)$, but had high total biomass $BM(0)$ and low fraction of M biomass $\phi_M(0)$. The reason for strong correlations between $P(T)$ and the two non-heritable determinants became clear by examining community dynamics. We had chosen maturation time so that Resource was in excess to avoid stationary phase. Thus, when a Newborn started with a higher-than-average total biomass (dotted lines in top panels of Figure S24),

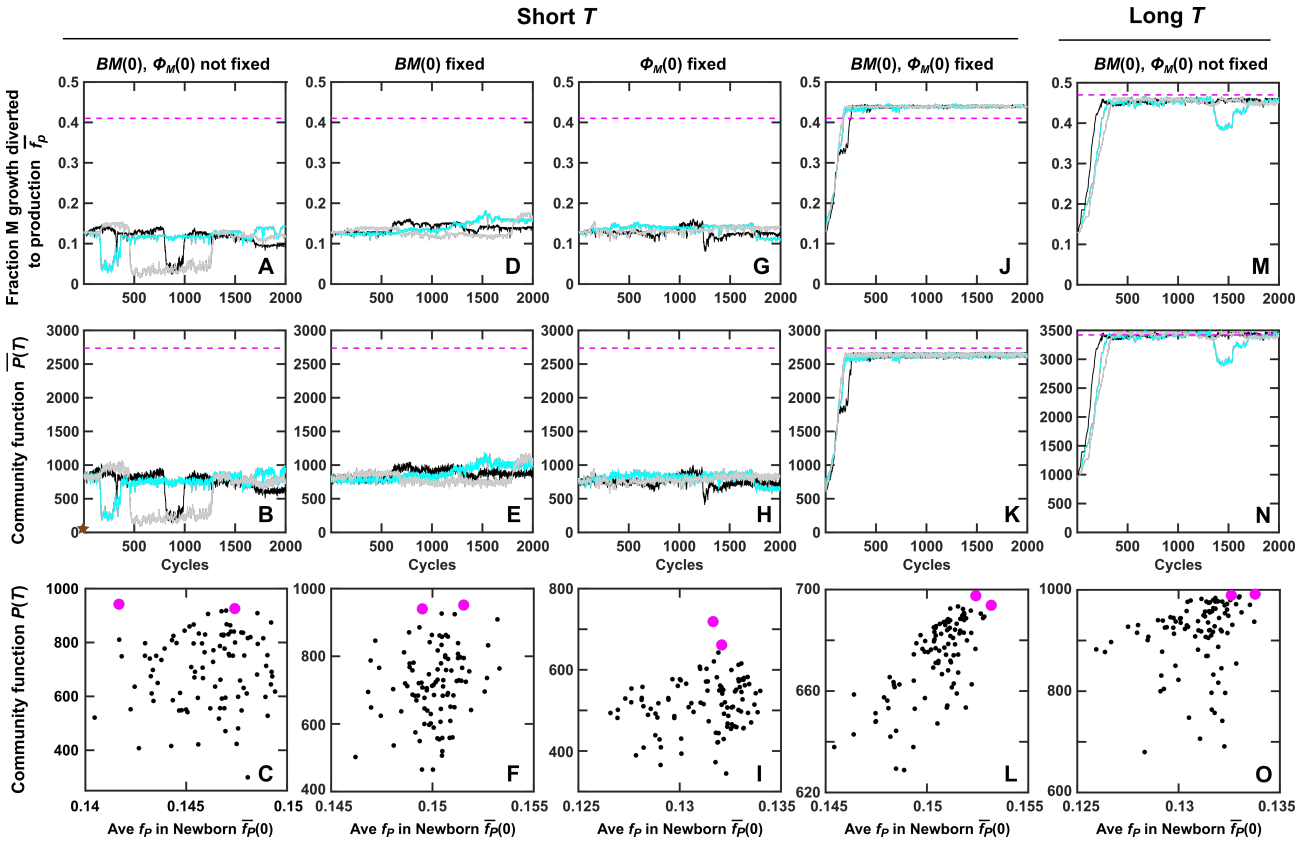

Figure 6: **Community selection succeeds when controlling the right experimental variables.** (**A-H**) Dynamics of selected communities at short maturation time T ($T = 17$, where on average 60% Resource is consumed by the end of T to avoid stationary phase). The growth parameters of H and M are fixed at upper bounds, and f_P starts at $f^*_{P,\,Mono} = 0.13$ (Figure S21B). (**A-C**) $BM(0)$ and $\phi_M(0)$ are allowed to fluctuate around $BM_{target} = 100$ and $\phi_M(T)$ of the previous cycle (e.g. pipetting and diluting a portion of the selected Adult into Newborns). (**J-L**) $BM(0)$ and $\phi_M(0)$ are fixed to $BM_{target} = 100$ and $\phi_M(T)$ of the previous cycle (e.g. sorting a fixed H biomass and M biomass into Newborns). This allows community function to improve. (**D-I**) Fixing either $BM(0)$ or $\phi_M(0)$ does not significantly improve community selection. (**M-O**) Selection dynamics at longer $T = 20$. Community function improves under selection even without fixing $BM(0)$ or $\phi_M(0)$. Magenta dashed lines: f^*_P optimal for $P(T)$ and maximal $P^*(T)$ when all five growth parameters are fixed at their upper bounds and $\phi_M(0)$ is optimal for community function. Black, cyan and gray curves are three independent simulation trials. $\overline{P}(T)$ is averaged across the two selected Adults and has the unit of $\widetilde{r}_P$, and $\overline{f}_P$ is obtained by averaging within each selected Adult and then averaging across the two selected Adults.

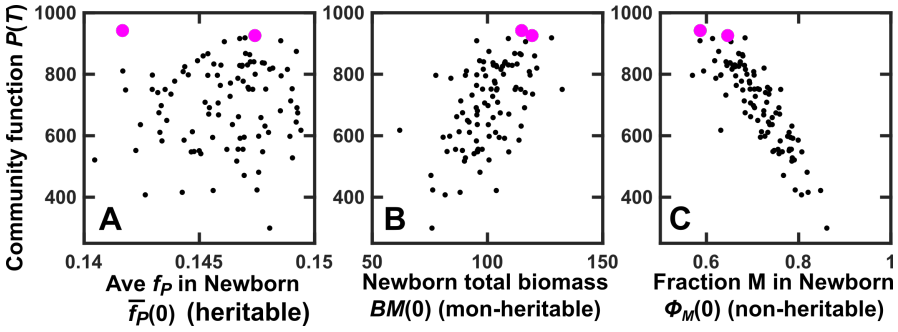

Figure 7: **When community selection is ineffective, community function correlates weakly with its heritable determinant and strongly with non-heritable determinants.** From community selection simulation, we randomly chose a selection cycle where 100 Newborns matured into 100 Adults. We plotted community function $P(T)$ of each Adult against characteristics of its corresponding Newborn community that determine community function. Each dot represents one community, and the two magenta dots indicate the two "successful" Newborns that achieved the highest community function at adulthood. (**A**) $P(T)$ only weakly correlates with $\overline{f}_P(0)$ (f_P averaged over all M individuals in a Newborn). (**B-C**) $P(T)$ strongly correlates with Newborn total biomass $BM(0)$ and Newborn fraction of M biomass $\phi_M(0)$.

higher-than-average M biomass would more thoroughly convert Resource (and Byproduct) to Product. Similarly, if a Newborn started with higher-than-average fraction of H biomass (dotted lines in bottom panels of Figure S24), then H would produce higher-than-average Byproduct which meant that M would endure a shorter growth lag, and make more Product.

In summary, variation in community function was dominated by variations in non-heritable determinants including Newborn total biomass $BM(0)$ and fraction of M biomass $\phi_M(0)$. This interfered with selection on $\overline{f}_P(0)$, the heritable determinant of community function. Consequently, selection failed to improve $P(T)$ (Figure 6B).

Reducing non-heritable variations promotes artificial community selection

Reducing non-heritable variations in community function should enable community selection to work. One possibility is to reduce the stochastic fluctuations in non-heritable determinants $BM(0)$ and $\phi_M(0)$. Indeed, when each Newborn received a fixed biomass of H and M (Methods, Section 6), $P(T)$ became strongly correlated with $\overline{f}_P(0)$ (Figure 6L). In this case, both $\overline{f}_P$ and community function $P(T)$ improved under selection (Figure 6, J and K) to near the optimal. Note that allocating a fixed biomass of fluorescent cells to Newborn communities could be experimentally realized by using a cell sorter since biomass scales with fluorescence intensity [35]. $P(T)$ improvement was not seen if either Newborn total biomass or species fraction was allowed to fluctuate stochastically (Figure 6, D-I). $P(T)$ also improved (Figure S25) if fixed numbers of H and M cells (instead of biomass) were allocated into each Newborn (Methods, Section 6).

Non-heritable variations in $P(T)$ could also be curtailed by reducing the dependence of $P(T)$ on non-heritable determinants. For example, we could extend the maturation time T to nearly deplete Resource. In this selection regimen, Newborns would still experience stochastic fluctuations in Newborn total biomass $BM(0)$ and fraction of M biomass $\phi_M(0)$. However all communities would end up with

similar $P(T)$ since "unlucky" communities would have time to "catch up" as "lucky" communities wait in stationary phase. Indeed, with extended T, community function improved without having to fix $BM(0)$ or $\phi_M(0)$ (Figure 6, M and N). However, stochastic fluctuations in $BM(0)$ and $\phi_M(0)$ could still cause non-heritable variations in community function by causing stochastic fluctuations in, for example, the duration of stationary phase (and thus cell survival or the length of recovery time).

As expected, the effectiveness of community selection depends on the uncertainty of community function measurements - another source of non-heritable variations. To test how measurement uncertainty affects community selection, we added to each $P(T)$ a random number drawn from a normal distribution with mean of zero and standard deviation of 5% of the ancestral $P(T)$. In this case, when we fixed $BM(0)$ and $\phi_M(0)$, community function improved, although at a slower rate than no measurement uncertainty (compare Figure S31 left panel with Figure 6 J & K). When measurement uncertainty doubled to 10%, community selection failed (Figure S31 right panel). Thus, multiple measurements of community function to reduce measurement uncertainty can make community selection more effective.

In summary, non-heritable variations in community function must be sufficiently suppressed for community selection to work. During community selection, seemingly innocuous experimental procedures such as pipetting could be problematic, and a more precise procedure such as cell sorting might be required. Our conclusions held when we used a different mutation rate (2×10^{-5} instead of 2×10^{-3} mutation per cell per generation per phenotype, Figure S26), a different distribution of mutation effects (a non-null mutation increased or decreased f_P by on average 2%, Figure S27), or incorporating epistasis (a non-null mutation would likely reduce f_P if the current f_P was high, and enhance f_P if the current f_P was low; Figure S28; Figure S9; Methods Section 5). Our conclusions also hold when improved growth parameters can reduce community function (Figure S14). We have also modeled a mutualistic H-M community where Byproduct was inhibitory to H. Thus, H benefited M by providing Byproduct, and M benefited H by removing Byproduct, similar to the syntrophic community of *Desulfovibrio vulgaris* and *Methanococcus maripaludis* [36]. We obtained similar conclusions in this mutualistic H-M community (Figure S30). Thus, our conclusions seem general.

Discussions

How might we improve functions of multi-species microbial communities via artificial selection? A common approach is to identify the appropriate combination of species types [8, 9, 12, 11, 15]. However, if we solely rely on species types, then without a constant influx of new species, community function will likely level off quickly [10]. Here, we consider artificial selection of communities with defined member species so that community function improves by new genotypes, particularly new genotypes that reduce individual growth rate and are thus disfavored by natural selection.

Pre-optimizing member species in monocultures may not lead to maximal community function due to difficulties in recapitulating community dynamics in monocultures. For example, we could start with H and M with all growth parameters at respective upper bounds, since within our parameter ranges, improving H and M growth generally improves community function (Figures S12 and S16). We could then improve M's f_P by group selection (Figure S1B). Specifically, we could start with n_{tot} of 100 Newborn M groups, each inoculated with one M cell (to facilitate group selection, Figure S1B bottom panel) [37]. We would supply each Newborn M group with the same amount of Resource as we would for H-M communities. Since it is difficult to reproduce community Byproduct dynamics in M groups, for simplicity we would supply excess Byproduct to Newborn M groups [1]. f_P optimal for monoculture

[1]Since Newborn groups start with a single M individual, artificial group selection here can also be viewed as artificial

$P(T)$ occurred at an intermediate value ($f^*_{P,\,Mono} = 0.13$; Figure S21). Consistent with this calculation, in simulations of M-group selection, f_P gradually increased to $f^*_{P,\,Mono} = 0.13$ (Figure S22). However, f_P optimal for monoculture $P(T)$ is much lower than f_P optimal for community $P(T)$ (Figure 5; see Methods Section 8 for an explanation).

Artificial selection of whole communities to improve a costly community function requires careful considerations on species choice (Figure 4), mutation rate, the total number of communities under selection, Newborn target total biomass, the amount of Resource added to each Newborn, and maturation time, as we have described in "Parameters of selection regimen". In addition, how we pre-grow M cells in preparation for inoculating Newborn communities for the first cycle can also affect community selection. Suppose that we grow up one master culture from a single cell over 23 generations (to a population size of $\sim 10^7$ which generates enough turbidity in 1-mL cultures) where mutations in f_P can occur during any time, and distribute ~60 cells into each of 100 Newborns. Then, there is a ~17% chance that all Newborns would contain at least 1 non-producing M cell. In contrast, if we grow up 100 cultures, and use one culture to inoculate one Newborn, then this chance reduces below 0.01%. However, these two arrangements resulted in almost identical evolutionary dynamics of average f_P and $P(T)$ (Figure S32).

In certain regards, community selection is similar to selection of mono-species groups. Group selection, and in a related sense, kin selection [38, 39, 40, 41, 42, 43, 44, 45, 46, 47, 48, 49, 50, 51, 52], have been extensively examined to explain, for example, the evolution of traits that lower individual fitness (e.g. sterile ants) but increase the success of a group [2]. In both group selection and community selection, Newborn size must not be too large [37, 58] and maturation time must not be too long. Otherwise, all entities (groups or communities) will accumulate non-producers in a similar fashion, and this low inter-entity variation impedes selection (Price equation [59]; Figure S1).

Community selection and group selection differ in two aspects. First, species interactions in a community could drive species composition to a value sub-optimal for community function ([60]). This problem does not exist for group selection especially when a group does not differentiate into interacting subgroups. Second, in group selection, when a Newborn group starts with a small number of individuals, a fraction of Newborn groups of the next cycle will show high heredity to the original Newborn group (Figure S1B, bottom panel). This facilitates group selection. In contrast, when a Newborn community starts with a small number of total individuals, large stochastic fluctuations in Newborn composition can interfere with community selection (Figure 6). In the extreme case, a member species may even be lost by chance. Even if a fixed biomass of each species is sorted into Newborns, heredity is much reduced in community selection due to random sampling of genotypes from member species [3].

Although suppressing non-heritable variations in a trait will always increase selection efficacy, here we show that for community selection, large non-heritable variations in community function can readily arise during routine experimental procedures such as pipetting. For example, at a target total biomass of 100 (~70 cells of average biomass 1.5) and excess Resource, pipetting a volume of an Adult to

individual selection where the trait under selection is an individual M's ability to make Product over time T as the individual grows into a population.

[2] Group selection is often applied in a broader sense to spatially-structured populations to explain the evolution of cooperative traits [53, 54]. In these cases, individuals form groups. Within each cycle, individuals grow based on their genotype (e.g. cooperators or cheaters) and group environment (cooperator-dominated or cheater-dominated). At the end of each cycle, individuals migrate among groups. However, if there are no births or deaths of groups, then selection acts on individuals instead of on groups [55, 56, 57].

[3] For example, if Newborn groups are initiated with a single cooperator and if the highest-functioning Adult group has accumulated 50% cheaters, then 50% Newborns of the next cycle will be initiated with a single cooperator. In contrast, if a Newborn community starts with a single cooperator from each of the two species and if the highest-functioning Adult has accumulated 50% cheaters in each species, then only 50%×50%= 25% Newborns of the next cycle will be initiated with pure cooperators.

seed a Newborn could already introduce non-heritable variations in community function (Figure 7B-C) sufficiently large to impede selection (Figure 6A-B). In contrast, if each Newborn received a fixed biomass of each species (via cell sorting for example), then community function rapidly improved (Figure 6J and K). If maturation time T was extended so that Resource would on average be nearly depleted by the end of T, then community function also improved (Figure 6M and N), provided that variations in stationary phase duration would not generate large, non-heritable variations in community function. Similar conclusions hold when we varied model assumptions by using a lower mutation rate (Figure S26), employing a different distribution of mutation effects (Figure S27), considering epistatsis (Figure S28), and modeling mutualistic H-M communities (Figure S30).

In the work of [8], authors tested two selection regimens with Newborn sizes differing by 100-fold. The authors hypothesized that smaller Newborns would have a high level of variation which should facilitate selection. However, the hypothesis was not corroborated by experiments, and as a possible explanation, the authors invoked the "butterfly effect" (the sensitivity of chaotic systems to initial conditions). Our results suggest that even for non-chaotic systems like the H-M community, selection could fail due to interference from non-heritable variations. This is because in Newborns with small sizes, fluctuations in community composition can be large, which compromises heritability of community trait.

A general ramification of our theory is that before launching a selection experiment, one should experimentally evaluate non-heritable variations in community function. One could initiate replicate Newborns using the most precise method (e.g. via cell sorting). Even at identical initial conditions, some levels of non-heritable variations in community function are inevitable. These can be caused by, for example, non-genetic phenotypic variations among cells [61], stochasticity in cell birth and death, and noise in community function measurements. If "noises" (variations among replicate communities) are small compared to "signals" (variations among communities with different levels of community function), then one can test less precise procedures (e.g. cell culture pipetting during community reproduction).

Microbes can co-evolve with each other and with their host in nature [62, 63, 64]. Some have proposed that complex microbial communities such as the gut microbiota could serve as a unit of selection [14]. Our work suggests that if selection for a costly microbial community function should occur in nature, then mechanisms for suppressing non-heritable variations in community function should be in place.

Methods

1 Equations

H, the biomass of H, changes as a function of growth and death,

$$\frac{dH}{dt} = g_H(\hat{R})H - \delta_H H \tag{1}$$

Grow rate g_H depends on the level of Resource $\hat{R}$ (hat $\hat{}$ representing pre-scaled value) as described by the Monod growth model (Figure S4)

$$g_H(\hat{R}) = g_{Hmax}\frac{\hat{R}}{\hat{R} + \hat{K}_{HR}}$$

where $\hat{K}_{HR}$ is the $\hat{R}$ at which $g_{Hmax}/2$ is achieved. δ_H is the death rate of H. Note that since Waste is in excess, Waste level does not change and thus does not enter the equation.

M, the biomass of M, changes as a function of growth and death,

$$\frac{dM}{dt} = (1 - f_P)\, g_M(\hat{R},\, \hat{B})M - \delta_M M \tag{2}$$

Total potential growth rate of M g_M depends on the levels of Resource and Byproduct ($\hat{R}$ and $\hat{B}$) according to the Mankad-Bungay model [25] due to its experimental support (Figure S5):

$$g_M(\hat{R},\, \hat{B}) = g_{Mmax} \frac{\hat{R}_M \hat{B}_M}{\hat{R}_M + \hat{B}_M} \left(\frac{1}{\hat{R}_M + 1} + \frac{1}{\hat{B}_M + 1} \right)$$

where $\hat{R}_M = \hat{R}/\hat{K}_{MR}$ and $\hat{B}_M = \hat{B}/\hat{K}_{MB}$ (Figure S4). $1 - f_P$ fraction of M growth is channeled to biomass increase. f_P fraction of M growth is channeled to making Product:

$$\frac{d\hat{P}}{dt} = \tilde{r}_P f_P g_M(\hat{R},\, \hat{B})M \tag{3}$$

where $\tilde{r}_P$ is the amount of Product made at the cost of one M biomass (tilde $\sim$ representing scaling factor, see below and Table 1).

Resource $\hat{R}$ is consumed proportionally to the growth of M and H; Byproduct $\hat{B}$ is released proportionally to H growth and consumed proportionally to M growth:

$$\frac{d\hat{R}}{dt} = -\hat{c}_{RM} g_M(\hat{R},\, \hat{B})M - \hat{c}_{RH} g_H(\hat{R})H \tag{4}$$

$$\frac{d\hat{B}}{dt} = \tilde{r}_B g_H(\hat{R})H - \hat{c}_{BM} g_M(\hat{R},\, \hat{B})M \tag{5}$$

Here, $\hat{c}_{RM}$ and $\hat{c}_{RH}$ are the amounts of $\hat{R}$ consumed per potential M biomass and H biomass, respectively. $\hat{c}_{BM}$ is the amount of $\hat{B}$ consumed per potential M biomass. $\tilde{r}_B$ is the amount of $\hat{B}$ released per H biomass grown. Our model assumes that Byproduct or Product is generated proportionally to H or M biomass grown, which is reasonable given the stoichiometry of metabolic reactions and experimental support [65]. The volume of community is set to be 1, and thus cell or metabolite quantities (which are considered here) are numerically identical to cell or metabolite concentrations.

In equations above, scaling factors are marked by "$\sim$", and will become 1 after scaling. Variables and parameters with hats will be scaled and lose their hats afterwards. Variables and parameters without hats will not be scaled. We scale Resource-related variable ($\hat{R}$) and parameters ($\hat{K}_{MR}$, $\hat{K}_{HR}$, $\hat{c}_{RM}$, and $\hat{c}_{RH}$) against $\tilde{R}(0)$ (Resource supplied to Newborn), Byproduct-related variable ($\hat{B}$) and parameters ($\hat{K}_{MB}$ and $\hat{c}_{BM}$) against $\tilde{r}_B$ (amount of Byproduct released per H biomass grown), and Product-related variable ($\hat{P}$) against $\tilde{r}_P$ (amount of Product made at the cost of one M biomass). For biologists who usually think of quantities with units, the purpose of scaling (and getting rid of units) is to reduce the number of parameters. For example, H biomass growth rate can be re-written as:

$$\begin{aligned} g_H(\hat{R}) &= g_{Hmax} \frac{\hat{R}}{\hat{R} + \hat{K}_{HR}} \\ &= g_{Hmax} \left(\frac{\hat{R}}{\tilde{R}(0)} \right) \Big/ \left(\frac{\hat{R}}{\tilde{R}(0)} + \frac{\hat{K}_{HR}}{\tilde{R}(0)} \right) \\ &= g_{Hmax} \frac{R}{(R + K_{HR})} \\ &= g_H(R) \end{aligned}$$

where $R = \hat{R}/\widetilde{R}(0)$ and $K_{HR} = \hat{K}_{HR}/\widetilde{R}(0)$. Thus, the unscaled $g_H(\hat{R})$ and the scaled $g_H(R)$ share identical forms. After scaling, the value of $\widetilde{R}(0)$ becomes irrelevant (1 with no unit). Similarly, since $\hat{R}_M = \frac{\hat{R}}{\widetilde{R}(0)} \Big/ \frac{\hat{K}_{MR}}{\widetilde{R}(0)} = \frac{R}{K_{MR}} = R_M$ and $\hat{B}_M = \frac{\hat{B}}{\widetilde{r}_B} \Big/ \frac{\hat{K}_{MB}}{\widetilde{r}_B} = \frac{B}{K_{MB}} = B_M$, $g_M(\hat{R},\, \hat{B}) = g_M(R,\, B)$.

Thus, scaled equations are

$$\frac{dH}{dt} = g_H(R)H - \delta_H H \tag{6}$$

$$\frac{dM}{dt} = (1 - f_P)\, g_M(R,\, B)M - \delta_M M \tag{7}$$

$$\begin{aligned} \frac{dP}{dt} &= \frac{d\hat{P}}{\widetilde{r}_P dt} \\ &= f_P g_M(\hat{R},\, \hat{B})M \\ &= f_P g_M(R,\, B)M \end{aligned} \tag{8}$$

$$\begin{aligned} \frac{dR}{dt} &= \frac{d\hat{R}/\widetilde{R}(0)}{dt} \\ &= -\frac{\hat{c}_{RM}}{\widetilde{R}(0)} g_M(\hat{R},\, \hat{B})M - \frac{\hat{c}_{RH}}{\widetilde{R}(0)} g_H(\hat{R})H \\ &= -c_{RM} g_M(R,\, B)M - c_{RH} g_H(R)H \end{aligned} \tag{9}$$

$$\begin{aligned} \frac{dB}{dt} &= \frac{d\hat{B}/\widetilde{r}_B}{dt} \\ &= g_H(\hat{R})H - \frac{\hat{c}_{BM}}{\widetilde{r}_B} g_M(\hat{R},\, \hat{B})M \\ &= g_H(R)H - c_{BM} g_M(R,\, B)M \end{aligned} \tag{10}$$

We have not scaled time here, although time can also be scaled by, for example, the community maturation time. Here, time has the unit of unit time (e.g. hr), and to avoid repetition, we often drop the time unit. After scaling, values of all parameters (including scaling factors) are in Table 1, and variables in our model and simulations are summarized in Table 2.

For this H-M community, the species ratio at time T at can be estimated in the following manner.

From Eq. 10:

$$\int_0^T \frac{dB}{dt} dt = \int_0^T g_H(R)H dt - \int_0^T c_{BM} g_M(R,\, B)M dt. \tag{11}$$

If we approximate Eq. 6-7 by ignoring the death rates so that $\frac{dH}{dt} \approx g_H(R)H$ and $\frac{dM}{dt} \approx (1 - f_P)\, g_M(R,\, B)M$, Eq. 11 becomes

$$B(T) \approx \int_0^T \frac{dH}{dt} dt - \frac{c_{BM}}{1 - f_P} \int_0^T \frac{dM}{dt} dt. \tag{12}$$

If B is the limiting factor for the growth of M so that B is mostly depleted, we can approximate $B \approx 0$. If T is large enough so that both M and H has multiplied significantly and $H(T) \gg H(0)$ and $M(T) \gg M(0)$, Eq. 12 becomes

$$H(T) - H(0) - \frac{c_{BM}}{1-f_P}\left(M(T) - M(0)\right) \approx H(T) - \frac{c_{BM}}{1-f_P}M(T) \approx 0,$$

the M:H ratio at time T is

$$\frac{M(T)}{H(T)} \approx \frac{1-f_P}{c_{BM}}. \tag{13}$$

If Newborn inherits parent Adult's ϕ_M, then the steady state $\phi_{M,SS}$ is

$$\phi_{M,SS} \approx \frac{1-f_P}{1-f_P+c_{BM}}. \tag{14}$$

In our simulations, because we supplied the H-M community with abundant R to avoid stationary phase, H grows almost at the maximal rate through T and releases B. If f_P is not too large ($f_P < 0.4$), which is satisfied in our simulations, M grows at a maximal rate allowed by B and keeps B at a low level. Thus, Eq. 14 is applicable and predicts the steady-state $\phi_{M,SS}$ well (see Figure S7). Note that significant deviation occurs when $f_P > 0.4$. This is because when f_P is large, M's biomass does not grow fast enough to deplete B so that we cannot approximate $B(T) \approx 0$ anymore.

2 Parameter choices

Our parameter choices are based on experimental measurements from a variety of organisms. Additionally, we choose growth parameters (maximal growth rates and affinities for metabolites) of ancestral and evolved H and M so that 1) the two species can coexist for a range of f_P during evolution and 2) improving all growth parameters up to their evolutionary upper bounds generally improves community function (Methods Section 3). This way, we could start with communities of H and M whose growth parameters are already maximized ("growth-adapted"), since mutations that reduce growth parameters will be selected against by both natural selection and community selection. In other words, only f_P can mutate, and higher f_P will be favored by community selection but disfavored by natural selection. With only one mutable parameter (f_P), we can identify the optimal f_P* associated with maximal community function (Figure 5). Evolutionary modeling is also greatly simplified.

For ancestral H, we set $g_{Hmax} = 0.25$ (equivalent to 2.8-hr doubling time if we choose hr as the time unit), $K_{HR} = 1$ and $c_{RH} = 10^{-4}$ (both with unit of $\widetilde{R}(0)$) (Table 1). This way, ancestral H can grow by about 10-fold by the end of $T = 17$. These parameters are biologically realistic. For example, for a *lys-S. cerevisiae* strain with lysine as Resource, un-scaled Monod constant is $\hat{K} = 1$ μM, and consumption $\hat{c}$ is 2 fmole/cell (Ref. [24], Figure 2 Source Data 1; bioRxiv). Thus, if we choose 10 μL as the community volume $\hat{V}$ and 2 μM as the initial Resource concentration, then $\widetilde{R}(0) = 2 \times 10^4$ fmole. After scaling, $K = \hat{K}\hat{V}/\widetilde{R}(0) = 0.5$ and $c = \hat{c}/\widetilde{R}(0) = 10^{-4}$, similar to values in Table 1.

To ensure the coexistence of H and M, M must grow faster than H for part of the maturation cycle. Since we have assumed M and H to have the same affinity for R (Table 1), g_{Mmax} must exceed g_{Hmax} (Figure 1), and M's affinity for Byproduct ($1/K_{MB}$) must be sufficiently large. Moreover, Byproduct consumed per Manufacturer biomass must be neither too small nor too large so that the steady state M:H is not extreme. Thus for ancestral M, we choose $g_{Mmax} = 0.58$ (equivalent to a doubling time of 1.2 hrs). We set $c_{BM} = \frac{1}{3}$ (units of r_B), meaning that Byproduct released during one H biomass growth is sufficient to generate 3 M biomass, which is biologically achievable ([23, 66]). When we choose $K_{MB} = \frac{5}{3} \times 10^2$

	Definition	Ancestral	Evolved
$\widetilde{r}_B$	amount of $\hat{B}$ released per H biomass grown	scaling factor, 1	no change
$\widetilde{r}_P$	amount of $\hat{P}$ released at the cost of one M biomass	scaling factor, 1	no change
$\widetilde{R}(0)$	initial amount of Resource in Newborn	scaling factor, 1	
f_P	fraction of M growth diverted to producing P	0.10	0.13#
K_{MR}	fold of $\widetilde{R}(0)$ at which $g_{Mmax}/2$ is achieved in excess B	1	$1/3$*
K_{MB}	amount of $\hat{B}$ at which $g_{Mmax}/2$ is achieved in excess R, scaled against $\widetilde{r}_B$	$\frac{5}{3} \times 10^2$	$\frac{1}{3} \times 10^2$*
K_{HR}	fold of $\widetilde{R}(0)$ at which $g_{Hmax}/2$ is achieved	1	$1/5$*
g_{Mmax}	maximal biomass growth rate of M	0.58/unit time	0.7*
g_{Hmax}	maximal biomass growth rate of H	0.25/unit time	0.3*
δ_M	death rate of M	3.5×10^{-3}/unit time	no change
δ_H	death rate of H	1.5×10^{-3}/unit time	no change
c_{RM}	fraction of $\widetilde{R}(0)$ consumed per M biomass grown	10^{-4}	no change
c_{RH}	fraction of $\widetilde{R}(0)$ consumed per H biomass grown	10^{-4}	no change
c_{BM}	amount of $\hat{B}$ consumed per M biomass grown, scaled against $\widetilde{r}_B$	$\frac{1}{3}$	no change
P_{mut}	mutation probability per cell division for each mutable phenotype	$2 \times 10^{-5} \sim 2 \times 10^{-3}$	

Table 1: Parameters for ancestral and evolved (growth- and mono-adapted) H and M. Parameters in the "Ancestral" column are used for Figure S12, while those in the "Evolved" column are used for all other figures. For maximal growth rates, * represents evolutionary upper bound. For $K_{SpeciesMetabolite}$, * represents evolutionary lower bound, which corresponds to evolutionary upper bound for Species's affinity for Metabolite ($1/K_{SpeciesMetabolite}$). # is from Figure 5B. In Methods Section 2, we explain our parameter choices (including why we hold some parameters constant during evolution).

Symbols	Definition
$M(t)$, $H(t)$	The biomass of M or H in a community at time t
$BM(t) = M(t) + H(t)$	The total biomass in a community at time t
$\phi_M(t)$	The fraction of M biomass at time t
BM_{target}	Pre-set target total biomass of Newborns during community reproduction
$I_M(t)$, $I_H(t)$	The integer number of M or H cells in a community at time t
$\varphi_M(t)$	The fraction of M individuals at time t
$L_M(t)$, $L_H(t)$	The biomass (length) of an individual M or H cell at time t, ranged between 1 and 2
$P(t)$	The amount of Product P in a community at time t, scaled by $\widetilde{r}_P$
$R(t)$	The amount of Resource R in a community at time t, scaled by $\widetilde{R}(0)$
$B(t)$	The amount of Byproduct B in a community at time t, scaled by $\widetilde{r}_B$
n_{dil}	The fold dilution when reproducing an Adult community
n_{tot}	Total number of communities under selection
T	Community maturation time, corresponding to the duration of a selection cycle

Table 2: A summary of variables used in the simulation.

(units of $\widetilde{r}_B$), H and M can coexist for a range of f_P (Figure 1). This value is biologically realistic. For example, suppose that H releases hypoxanthine as Byproduct. A hypoxanthine-requiring *S. cerevisiae* M strain evolved under hypoxanthine limitation could achieve a Monod constant for hypoxanthine at 0.1 μM (bioRxiv). If the volume of the community is 10 μL, then $K_{MB} = \frac{5}{3} \times 10^2$ (units of $\widetilde{r}_B$) corresponds to an absolute release rate $\widetilde{r}_B = 0.1\,\mu M \times 10\mu\text{L}/(\frac{5}{3} \times 10^2) = 6$ fmole per releaser biomass born. At 8 hour doubling time, this translates to 6 fmole/(1 cell$\times$8 hr)≈ 0.75 fmole/cell/hr, within the ballpark of experimental observation (~0.3 fmole/cell/hr, bioRxiv). As a comparison, a lysine-overproducing yeast strain reaches a release rate of 0.8 fmole/cell/hr (bioRxiv) and a leucine-overproducing strain reaches a release rate of 4.2 fmole/cell/hr ([66]). Death rates δ_H and δ_M are chosen to be 0.5% of H and M's respective upper bound of maximal growth rate, which are within the ballpark of experimental observations (e.g. the death rate of a *lys-* strain in lysine-limited chemostat is 0.4% of maximal growth rate, bioRxiv).

We assume that H and M consume the same amount of R per new cell ($c_{RH} = c_{RM}$) since the biomass of various microbes share similar elemental (e.g. carbon or nitrogen) compositions [67]. Specifically, $c_{RH} = c_{RM} = 10^{-4}$ (units of $\widetilde{R}(0)$), meaning that input Resource can yield a maximum of 10^4 total biomass.

In initial simulations, growth parameters (maximal growth rates g_{Mmax} and g_{Hmax} and affinities for nutrients $1/K_{MR}$, $1/K_{MB}$, and $1/K_{HR}$) and production cost parameter ($f_P \in [0,\,1]$) are allowed to change during evolution, since these phenotypes have been observed to rapidly evolve within tens to hundreds of generations ([27, 28, 29, 30]). For example, several-fold improvement in nutrient affinity [28] and ~20% increase in maximal growth rate [30] have been observed in experimental evolution. Thus we allow affinities $1/K_{MR}$, $1/K_{HR}$, and $1/K_{MB}$ to increase by 3-fold, 5-fold, and 5-fold respectively, and allow g_{Hmax} and g_{Mmax} to increase by 20%. These bounds also ensure that evolved H and M can coexist for $f_p < 0.5$, and that Resource is on average not depleted by T to avoid cells entering stationary phase. Although maximal growth rate and nutrient affinity can sometimes show trade-off (e.g. Ref. [28]), for simplicity we assume here that they are independent of each other. We hold metabolite consumption (c_{RM}, c_{BM}, c_{RH}) constant because conversion of essential elements such as carbon and nitrogen into biomass is unlikely to evolve quickly and dramatically, especially when these elements are not in large excess ([67]). Similarly, we hold the scaling factors $\widetilde{r}_P$ and $\widetilde{r}_B$ constant, assuming that they do not change rapidly during evolution due to stoichiometric constraints of biochemical reactions. We hold death rates (δ_M, δ_H) constant because they are much smaller than growth rates in general and thus any changes are likely inconsequential.

3 Choosing growth parameter ranges so that we can fix growth parameters to upper bounds

Improving individual growth (maximal growth rate and affinity for metabolites) does not always lead to improved community function (Figure S11). However, we have chosen H and M growth parameters so that improving them from their ancestral values up to upper bounds generally improves community function (see below). When Newborn communities are assembled from "growth-adapted" H and M with maximal growth parameters, two advantages are apparent.

First, after fixing growth parameters of H and M to their upper bounds, we can identify a locally maximal community function. Specifically, for a Newborn with total biomass $BM(0) = 100$ and fixed Resource R, we can calculate $P(T)$ under various f_P and $\phi_M(0)$. Since both numbers range between 0 and 1, we calculate $P(T,\, f_P = 0.01 \times i,\, \phi_M(0) = 0.01 \times j)$ for integers i and j between 1 and 99. There is a single maximum for $P(T)$ when $i = 41$ and $j = 54$. In other words, if M invests $f_P^* = 0.41$ of

its potential growth to make Product and if the fraction of M biomass in Newborn$\phi^*_M(0) = 0.54$, then maximal community function $P^*(T)$ is achieved (Figure 5A; magenta dashed line in Figure 6).

Second, growth-adapted H and M are evolutionarily stable in the sense that deviations (reductions) from upper bounds will reduce both individual fitness and community function, and are therefore disfavored by natural selection and community selection.

Below, we present evidence that within our parameter ranges (Table 1), improving growth parameters generally improves community function. When f_P is optimal for community function ($f^*_P = 0.41$), if we fix four of the five growth parameters to their upper bounds, then as the remaining growth parameter improves, community function increases (magenta lines in top panels of Figure S16). Moreover, mutants with a reduced growth parameter are out-competed by their growth-adapted counterparts (magenta lines in bottom panels of Figure S16).

When $f_P = f^*_{P,\,Mono} = 0.13$ (optimal for M-monoculture function in Figure 5B; the starting genotype for most community selection trials in this paper), community function and individual fitness generally increase as growth parameters improve (black dashed lines in Figure S16). However, when M's affinity for Resource ($1/K_{MR}$) is reduced from upper bound, fitness improves (black dashed line in Panel J, Figure S16). Mathematically speaking, this is a consequence of the Mankad-Bungay model [25] (Figure S5B). Let $R_M = R/K_{MR}$ and $B_M = B/K_{MB}$. Then,

$$\begin{aligned}\frac{\partial g_M}{\partial K_{MR}} &= \frac{\partial g}{\partial R_M}\frac{\partial R_M}{\partial K_{MR}} = \frac{\partial\left[g_{max}\frac{R_M B_M}{R_M+B_M}\left(\frac{1}{1+R_M}+\frac{1}{1+B_M}\right)\right]}{\partial R_M}\frac{\partial R_M}{\partial K_{MR}} = g_{max}\frac{-R_M}{K_{MR}}\left[\frac{B_M\left(R_M+B_M\right)-R_M B_M}{\left(R_M+B_M\right)^2}\right.\\ &= g_{max}\frac{R_M B_M}{\left(R_M+B_M\right)K_{MR}}\left(\frac{R_M}{(1+R_M)^2}-\frac{B_M}{R_M+B_M}\left(\frac{1}{1+R_M}+\frac{1}{1+B_M}\right)\right)\end{aligned}$$

If $R_M \ll 1 \ll B_M$ (corresponding to limiting R and abundant B),

$$\frac{R_M}{(1+R_M)^2}-\frac{B_M}{R_M+B_M}\left(\frac{1}{1+R_M}+\frac{1}{1+B_M}\right) \approx \frac{R_M}{(1+R_M)^2}-\frac{1}{1+R_M} = -\frac{1}{(1+R_M)^2} \qquad (15)$$

and thus $\frac{\partial g_M}{\partial K_{MR}} < 0$. This is the familiar case where growth rate increases as the Monod constant decreases (i.e. affinity increases). However, if $B_M \ll 1 \ll R_M$

$$\frac{R_M}{(1+R_M)^2}-\frac{B_M}{R_M+B_M}\left(\frac{1}{1+R_M}+\frac{1}{1+B_M}\right) \approx \frac{1}{R_M}-\frac{B_M}{R_M}\left(\frac{1}{1+B_M}\right) = \frac{1}{R_M(1+B_M)} \qquad (16)$$

and thus $\frac{\partial g_M}{\partial K_{MR}} > 0$. In this case, growth rate decreases as the Monod constant decreases (i.e. affinity increases). In other words, decreased affinity for the abundant nutrient improves growth rate. Transporter competition for membrane space [68] could lead to this result, since reduced affinity for abundant nutrient may increase affinity for rare nutrient. At all f_P, R is abundant and B is limiting at the beginning of each cycle (Eq. 16), and therefore M cells with lower affinity for R will grow faster than those with higher affinity (Figure S17). At the end of each cycle, the opposite is true (Figure S17). As f_P decreases, M has higher growth capacity, and thus the first stage of B limitation lasts longer. Consequently, M can gain higher overall fitness by lowering affinity for R (Figure S17A).

Regardless, decreased M affinity for Resource ($1/K_{MR}$) only leads to a very slight increase in M fitness (Figure S16J) and a very slight decrease in $P(T)$ (Figure S17B). Moreover, this only occurs at low f_P at the beginning of community selection, and thus may be neglected. Indeed, if we start all growth parameters at their upper bounds and $f_P = 0.13$, and perform community selection while allowing all

parameters to vary (Figure S18), then $1/K_{MR}$ decreases somewhat, yet the dynamics of f_P is similar to when we only allow f_P to change (compare Figure S18D with Figure 6A). Indeed, allowing both f_P and $1/K_{MR}$ to evolve does not change our conclusions as shown in Figure S19.

4 Mutation rate and the distribution of mutation effects

Literature values of mutation rate and the distribution of mutation effects are highly variable. Below, we briefly review the literature and discuss rationales of our choices.

Our "mutation rate" refers to the rate of mutations that either enhance a phenotype ("enhancing mutations") or diminish a phenotype ("diminishing mutations"). Enhancing mutations of maximal growth rate (g_{Hmax} and g_{Mmax}) and of nutrient affinity ($1/K_{HR}$, $1/K_{MR}$, $1/K_{MB}$) enhance the fitness of an individual ("beneficial mutations"). In contrast, enhancing mutations in f_p diminish the fitness of an individual ("deleterious mutations"). Among mutations, a fraction will be neutral in that they do not affect the phenotype of interest. For example, the vast majority of synonymous mutations are neutral [69]. A larger fraction of neutral mutations is equivalent to a lower rate of phenotype-altering mutations. However, experimentally, the fraction of neutral mutations is difficult to determine. Consider fitness as the phenotype of interest. Whether a mutation is neutral or not can vary as a function of effective population size, and selection condition. For example, at low population size due to genetic drift (i.e. changes in allele frequencies due to chance), a beneficial or deleterious mutation may not be selected for or selected against, and is thus neutral with respect to selection [70, 71]. Mutations in an antibiotic-degrading gene can be neutral under low antibiotic concentrations, but deleterious under high antibiotic concentrations [72].

Depending on the phenotype, the rate of phenotype-altering mutations is highly variable. Although mutations that cause qualitative phenotypic changes (e.g. drug resistance) occur at a rate of 10^{-8}~10^{-6} per genome per generation in bacteria and yeast [73, 74], mutations affecting quantitative traits such as growth rate occur much more frequently. For example in yeast, mutations that increase growth rate by $\geq 2\%$ occur at a rate of $\sim 10^{-4}$ per genome per generation (calculated from Figure 3 of Ref. [75]), and mutations that reduce growth rate occur at a rate of $10^{-4} \sim 10^{-3}$ per genome per generation [33, 76]. Moreover, mutation rate can be elevated by as much as 100-fold in hyper-mutators where DNA repair is dysfunctional [77, 78, 76]. Here for a mutable phenotype, we assume a high, but biologically feasible, rate of 2×10^{-3} phenotype-altering mutations per cell per generation to speed up computation. At this rate, an average community would sample ~20 new mutations per phenotype during maturation. We have also tried 100-fold lower mutation rate. As expected, evolutionary dynamics slows down, but all of our conclusions still hold (Figure S26).

Among phenotype-altering mutations, tens of percent create null mutants, as illustrated by experimental studies on protein, viruses, and yeast [31, 32, 33]. Thus, we assume that 50% of phenotype-altering mutations are null (i.e. zero maximal growth rate, zero affinity for metabolite, or zero f_P). Among non-null mutations, the relative abundances of enhancing versus diminishing mutations are highly variable in different experiments. It can be impacted by effective population size. For example, with a large effective population size, the survival rate of beneficial mutations is 1000-fold lower due to clonal interference (competition between beneficial mutations) [79]. The relative abundance of enhancing versus diminishing mutations also strongly depends on the starting phenotype [31, 72, 70]. For example with ampicillin as a substrate, the TEM-1 β-lactamase acts as a "perfect" enzyme. Consequently, mutations were either neutral or diminishing, and few enhanced enzyme activity [72]. In contrast with a novel substrate such as cefotaxime, the enzyme had undetectable activity, and diminishing mutations were not detected while 2% of tested mutations were enhancing [72]. When modeling H-M communities, we assume that the

ancestral H and M have intermediate phenotypes that can be enhanced or diminished.

We base our distribution of mutation effects on experimental studies where a large number of enhancing and diminishing mutants have been quantified in an unbiased fashion. An example is a study from the Dunham lab where the fitness effects of thousands of *S. cerevisiae* mutations were quantified under various nutrient limitations [34]. Specifically for each nutrient limitation, the authors first measured $\triangle s_{WT} = (w_{WT} - \bar{w}_{WT})/\bar{w}_{WT} = w_{WT}/\bar{w}_{WT} - 1$, the deviation in relative fitness of thousands of bar-coded wild-type control strains from the wild-type mean fitness. Due to experimental noise, $\triangle s_{WT}$ is distributed with zero mean and non-zero variance. Then, the authors measured thousands of $\triangle s_{MT}$, each corresponding to the relative fitness change of a bar-coded mutant strain with respect to the mean of wild-type fitness (i.e. $\triangle s_{MT} = (w_{MT} - \bar{w}_{WT})/\bar{w}_{WT}$). From these two distributions, we derive $\mu_{\Delta s}$, the probability density function (PDF) of relative fitness change caused by mutations $\Delta s = \triangle s_{MT} - \triangle s_{WT}$ (see Figure S8 for interpreting PDF), in the following manner.

First, we calculate $\mu_m(\triangle s_{MT})$, discrete PDF of mutant strain relative fitness change, with bin width 0.04. In other words, $\mu_m(\triangle s_{MT})$ =counts in the bin of $[\triangle s_{MT} - 0.02, \triangle s_{MT} + 0.02]$ / total counts/0.04 where $\triangle s_{MT}$ ranges from -0.6 and 0.6 which is sufficient to cover the range of experimental outcome. The Poissonian uncertainty of μ_m is $\delta\mu_m(\triangle s_{MT}) = \sqrt{\text{counts per bin}}$/total counts/0.04. Repeating this process for wild-type collection, we obtain PDF of wild-type strain relative fitness $\mu_w(\triangle s_{WT})$. Next, from $\mu_w(\triangle s_{WT})$ and $\mu_m(\triangle s_{MT})$, we derive $\mu_{\Delta s}(\Delta s)$, the PDF of Δs with bin width 0.04:

$$\mu_{\Delta s}(\Delta s = i \times 0.04) = 0.04 \times \sum_{j=-\infty}^{+\infty} \mu_w(j \times 0.04)\mu_m((i+j) \times 0.04). \tag{17}$$

assuming that $\triangle s_{MT}$ and $\triangle s_{WT}$ are independent from each other. Here, i is an integer from -15 to 15. The uncertainty for $\mu_{\Delta s}$ is calculated by propagation of error. That is, if f is a function of x_i (i = 1, 2, ..., n), then s_f, the error of f, is $s_f^2 = \sum \left(\frac{\partial f}{\partial x_i} s_{x_i}\right)^2$ where s_{x_i} is the error or uncertainty of x_i. Thus,

$$\delta\mu_{\Delta s}(i) = 0.04 \times \sqrt{\sum_j \left[(\delta\mu_w(j)\mu_m(i+j))^2 + (\mu_w(j)\delta\mu_m(i+j))^2\right]} \tag{18}$$

where $\mu_w(j)$ is short-hand notation for $\mu_w(\triangle s_{WT} = j \times 0.04)$ and so on. Our calculated $\mu_{\Delta s}(\Delta s)$ with error bar of $\delta\mu_{\Delta s}$ is shown in Figure S8.

Our reanalysis demonstrates that distributions of mutation fitness effects $\mu_{\Delta s}(\Delta s)$ are largely conserved regardless of nutrient conditions and mutation types (Figure S8B). In all cases, the relative fitness changes caused by beneficial (fitness-enhancing) and deleterious (fitness-diminishing) mutations can be approximated by separate exponential distributions with different means s_+ and s_-, respectively. After normalization to have a total probability of 1, we have:

$$\mu_{\Delta s}(\Delta s) = \begin{cases} \frac{1}{s_+ + s_-(1-\exp(-1/s_-))} \exp(-\Delta s/s_+) & \text{if } \Delta s \geq 0 \\ \frac{1}{s_+ + s_-(1-\exp(-1/s_-))} \exp(\Delta s/s_-) & \text{if } -1 < \Delta s < 0 \end{cases} \tag{19}$$

We fit the Dunham lab haploid data (since microbes are often haploid) to Eq. 19, using $\mu_{\Delta s}(i)/\delta\mu_{\Delta s}(i)$ as the weight for non-linear least squared regression (green lines in Figure S8B). We obtain $s_+ = 0.050 \pm 0.002$ and $s_- = 0.067 \pm 0.003$.

Interestingly, exponential distribution described the fitness effects of deleterious mutations in an RNA virus significantly well [31]. Based on extreme value theory, the fitness effects of beneficial mutations are predicted to follow an exponential distribution [80, 81], which has gained experimental support from bacterium and virus [82, 83, 84] (although see [85, 75] for counter examples). Evolutionary models based on exponential distributions of fitness effects have shown good agreements with experimental data [79, 86].

We have also simulated smaller average mutational effects based on measurements of spontaneous or chemically-induced (instead of deletion) mutations. For example, the fitness effects of nonlethal deleterious mutations in *S. cerevisiae* were mostly 1%~5% [33], and the mean selection coefficient of beneficial mutations in *E. coli* was 1%~2% [82, 79]. Thus, as an alternative, we choose $s_+ = 0.02$; $s_- = -0.02$, and obtain similar conclusions (Figure S27).

5 Modeling epistasis on f_P

Epistasis, where the effect of a new mutation depends on prior mutations ("genetic background"), is known to affect evolutionary dynamics. Epistatic effects have been quantified in various ways. Experiments on viruses, bacteria, yeast, and proteins have demonstrated that for two mutations that are both deleterious or random, viable double mutants experience epistatic effects that are nearly symmetrically distributed around a value near zero [87, 88, 89, 90, 91]. In other words, a significant fraction of mutation pairs show no epistasis, and a small fraction show positive or negative epistasis (i.e. a double mutant displays a stronger or weaker phenotype than expected from additive effects of the two single mutants). Epistasis between two beneficial mutations can vary from being predominantly negative [88] to being symmetrically distributed around zero [89]. Furthermore, a beneficial mutation tends to confer a lower beneficial effect if the background already has high fitness ("diminishing returns") [92, 89, 93].

A mathematical model by Wiser et al. incorporates diminishing returns epistasis [86]. In this model, beneficial mutations of advantage s in the ancestral background are exponentially distributed with probability density $\alpha \exp(-\alpha s)$, where $1/\alpha > 0$ is the mean advantage. After a mutation with advantage s has occurred, the mean advantage of the next mutation would be reduced to $1/[\alpha(1+gs)]$, where $g > 0$ is the "diminishing returns parameter". Wiser et al. estimates $g \approx 6$. This model quantitatively explains the fitness dynamics of evolving *E. coli* populations.

Based on the above experimental and theoretical literature, we model epistasis on f_P in the following manner. Let the relative mutation effect on f_P be $\Delta f_P = (f_{P,mut} - f_P)/f_P$ (note $\Delta f_P \geq -1$). Then, $\mu(\Delta f_P,\ f_P)$, the probability density function of Δf_P at the current f_P value, is described by a form similar to Eq. 19:

$$\mu(\Delta f_P,\ f_P) = \begin{cases} \frac{1}{s_+(f_P)+s_-(f_P)(1-\exp(-1/s_-(f_P)))} \exp(-\Delta f_P/s_+(f_P)) & \text{if } \Delta f_P \geq 0 \\ \frac{1}{s_+(f_P)+s_-(f_P)(1-\exp(-1/s_-(f_P)))} \exp(\Delta f_P/s_-(f_P)) & \text{if } -1 < \Delta f_P < 0 \end{cases} \quad (20)$$

Here, $s_+(f_P)$ and $s_-(f_P)$ are respectively the mean Δf_P for enhancing and diminishing mutations at current f_P. We assign $s_+(f_P) = s_{+init}/(1 + g \times (f_P/f_{P,init} - 1))$, where $f_{P,init}$ is the f_P of the initial background in a community selection trial (generally $f_{P,init} = f^*_{P,Mono} = 0.13$), s_{+init} is the mean enhancing Δf_P occurring in the initial background, and $0 < g < 1$ is the epistatic factor. Similarly, $s_-(f_P) = s_{-init} \times (1 + g \times (f_P/f_{P,init} - 1))$ is the mean $|\Delta f_P|$ for diminishing mutations at current f_P. In the initial background since $f_P = f_{P,init}$, we have $s_+(f_P) = s_{+init}$ and $s_-(f_P) = s_{-init}$ where $s_{+init} = 0.050$ and $s_{-init} = 0.067$ (Figure S8). For subsequent mutations, consistent with the diminishing returns principle, if current $f_P > f_{P,init}$, then a new enhancing mutation becomes less likely and its mean effect also becomes smaller, while a new diminishing mutation becomes more likely and its mean effect also becomes bigger (ensured by $g > 0$; Figure S9 right panel). Similarly, if current $f_P < f_{P,init}$, then a new enhancing mutation becomes more likely and its mean effect also becomes bigger, while a diminishing mutation becomes less likely and its mean effect also becomes smaller (ensured by $0 < g < 1$; Figure S9 left panel). In summary, our model captures not only diminishing returns epistasis, but also our understanding of mutational effects on protein stability [70].

6 Simulation code of community selection

Our simulations track the biomass and phenotypes of individual cells as well as the amounts of Resource, Byproduct, and Product in each community throughout community selection. Deterministic processes include cell biomass growth, cell division, and changes in chemical concentrations. Stochastic processes include cell death, mutation, and the partitioning of cells of a selected Adult community into Newborn communities. Briefly, a cell starts at a biomass of 1. Once cell biomass grows to the division threshold of 2, the cell divides into two equal halves. Thus, our simulations track continuous biomass increase (Figure S3) as well as discrete cell division events, capturing experimental observations of *E. coli* growth [26]. Cell death occurs stochastically during each time interval with a probability dictated by the death rate. Immediately after cell division, each new cell mutates with a probability equal to the mutation rate. A mutation changes one of the mutable phenotypes, with a probability of 0.5 of generating a null mutant (maximal growth rate, or affinity for a metabolite, or f_P=0) and a probability of 0.5 of increasing or decreasing the phenotype by a few percent (4). During community maturation, Resource R, Byproduct B, and Product P change due to consumption and release. After maturation time T, the Adult community with the highest function is chosen for reproduction where H and M cells are randomly distributed into Newborns of the next cycle. Simulation code is adjusted according to how community reproduction is implemented (e.g. pipetting or cell sorting). After the top-functioning Adult is depleted, the second top-functioning Adult is used until a total of n_{tot} Newborns are generated. We present details of the code below.

The code starts with a total of $n_{tot} = 100$ Newborn communities with identical configuration:

- each community has 100 total cells of biomass 1. Thus, total biomass $BM(0) = 100$.
- 40 cells are H. 60 cells are M with identical f_P. Thus, M biomass $M(0) = 60$ and fraction of M biomass $\phi_M(0) = 0.6$.

In our community selection simulations, unless otherwise stated, we do not model mutations arising during pre-growth prior to inoculating Newborns of the first cycle. For example, non-producing M cells can arise as a single M cell grows into a monoculture. If each Newborn community's 60 M cells are inoculated from a distinct population expanded from a single non-null M cell, then at least a fraction of Newborns will be free of null mutants (Figure S32). Adults matured from these Newborns will have high community functions and be chosen to reproduce. Thus, starting from the second cycle, community selection would be similar whether or not we consider mutants arising during pre-growth.

In the beginning, a random number is used to seed the random number generator for each Newborn community, and this number is saved so that the sequence of random numbers used below can be exactly repeated for data analysis. The initial amount of Resource is 1 unit of $\widetilde{R}(0)$, the initial Byproduct is $B(0) = 0.$ and the initial Product $P(0) = 0$. The cycle time is divided into time steps of $\Delta\tau = 0.05$.

Resource $R(t)$ and Byproduct $B(t)$ during time interval $[\tau,\ \tau + \Delta\tau]$ are calculated by solving the following equations (similar to Eqs. 9-10) within $[\tau, \tau + \Delta\tau]$ using the initial condition $R(\tau)$ and $B(\tau)$ via the ode23s solver in Matlab:

$$\frac{dR}{dt} = -c_{RM} g_M(R,\ B) M(\tau) - c_{RH} g_H(R) H(\tau) \tag{21}$$

$$\frac{dB}{dt} = g_H(R) H(\tau) - c_{BM} g_M(R,\ B) M(\tau) \tag{22}$$

where $M(\tau)$ and $H(\tau)$ are the biomass of M and H at time τ (treated as constants during time interval $[\tau,\ \tau + \Delta\tau]$), respectively. The solutions from Eq. 21 and 22 are used in the integrals below.

Suppose that H and M are rod-shaped organisms with a fixed diameter. Thus, the biomass of an H cell at time τ can be written as the length variable $L_H(\tau)$. The continuous growth of L_H during τ and $\tau + \Delta\tau$ can be described as

$$\frac{dL_H}{dt} = g_H(R)L_H$$

thus $L_H(\tau + \Delta\tau)$ is

$$\ln \frac{L_H(\tau + \Delta\tau)}{L_H(\tau)} = \int_{\tau}^{\tau+\Delta\tau} g_H(R)dt$$

and

$$L_H(\tau + \Delta\tau) = L_H(\tau) \exp\left(\int_{\tau}^{\tau+\Delta\tau} g_H(R)dt\right). \tag{23}$$

Similarly, let the length of an M cell be $L_M(\tau)$. The continuous growth of M can be described as

$$\frac{dL_M}{dt} = (1 - f_P)g_M(R,\, B)L_M.$$

Thus for an M cell, its length $L_M(\tau + \Delta\tau)$ is

$$L_M(\tau + \Delta\tau) = L_M(\tau) \exp\left(\int_{\tau}^{\tau+\Delta\tau} (1 - f_P)g_M(R,\, B)dt\right) \tag{24}$$

From Eq. 7 and 8, within $\Delta\tau$,

$$\begin{aligned}\frac{dP}{dt} &= f_P g_M(R,\, B)M \\ &\sim \frac{f_P}{1 - f_P}\frac{dM}{dt}\end{aligned}$$

and we get

$$P(\tau + \Delta\tau) = P(\tau) + \frac{f_P}{1 - f_P}\left(M(\tau + \Delta\tau) - M(\tau)\right)$$

where $M(\tau + \Delta\tau) = \sum L_M(\tau + \Delta\tau)$ is the sum of the lengths of all M cells at $\tau + \Delta\tau$.

At the end of each $\Delta\tau$, each H and M cell has a probability of $\delta_H\Delta\tau$ and $\delta_M\Delta\tau$ to die, respectively. This is simulated by assigning a random number between [0, 1] for each cell and those receive a random number less than $\delta_H\Delta\tau$ or $\delta_M\Delta\tau$ get eliminated. For surviving cells, if a cell's length ≥ 2, this cell will divide into two cells with half the original length.

After division, each cell has a probability of P_{mut} to acquire a mutation that changes each of its mutable phenotype (Methods, Section 4). As an example, let's consider mutations in f_P. If a mutation occurs, then f_P will be multiplied by $(1 + \Delta f_P)$, where Δf_P is determined as below.

First, a uniform random number u_1 between 0 and 1 is generated. If $u_1 \leq 0.5$, $\Delta f_P = -1$, which represents 50% chance of a null mutation ($f_P = 0$). If $0.5 < u_1 \leq 1$, Δf_P follows the distribution defined by Eq. 20 with $s_+(f_P) = 0.05$ for f_P-enhancing mutations and $s_-(f_P) = 0.067$ for f_P-diminishing mutations when epistasis is not considered (Methods, Section 4). In the simulation, Δf_P

is generated via inverse transform sampling. Specifically, $C(\Delta f_P)$, the cumulative distribution function (CDF) of Δf_P , can be found by integrating Eq. 19 from -1 to Δf_P:

$$\begin{aligned} C(\Delta f_P) &= \int_{-1}^{\Delta f_P} \mu_{\Delta s}(x)dx \\ &= \begin{cases} \frac{s_-}{s_+ + s_-(1-e^{-1/s_-})} \left(\exp(\Delta f_P/s_-) - \exp(-1/s_-)\right) & \text{if } \Delta f_P \le 0 \\ 1 - \frac{s_+}{s_+ + s_-(1-e^{-1/s_-})} \exp(-\Delta f_P/s_+) & \text{if } \Delta f_P \ge 0 \end{cases} \end{aligned} \tag{25}$$

The two parts of Eq. 25 overlap at $C(\Delta f_P = 0) = s_-(1 - e^{-1/s_-})/\left[s_+ + s_-(1 - e^{-1/s_-})\right]$.

In order to generate Δf_P satisfying the distribution in Eq. 19, a uniform random number u_2 between 0 and 1 is generated and we set $C(\Delta f_P) = u_2$. Inverting Eq. 25 yields

$$\Delta f_P = \begin{cases} s_- \ln\left(u_2(s_+ + s_-(1 - e^{-1/s_-}))/s_- + e^{-1/s_-}\right) & u_2 \le \frac{s_-(1-e^{-1/s_-})}{s_+ + s_-(1-e^{-1/s_-})} \\ -s_+ \ln\left((1 - u_2)(s_+ + s_-(1 - e^{-1/s_-}))/s_+\right) & u_2 > \frac{s_-(1-e^{-1/s_-})}{s_+ + s_-(1-e^{-1/s_-})} \end{cases} \tag{26}$$

When epistasis is considered, $s_+(f_P) = s_{+init}/(1 + g \times (f_P/f_{P,init} - 1))$ and $s_-(f_P) = s_{-init} \times (1 + g \times (f_P/f_{P,init} - 1))$ are used in Eq. 26 to calculated Δf_P for each cell with different current f_P (Methods Section 5).

If a mutation increases or decreases the phenotypic parameter beyond its bound (Table 1), the phenotypic parameter is set to the bound value.

The above growth/death/division/mutation cycle is repeated from time 0 to T. Note that since the size of each M and H cell can be larger than 1, the integer numbers of M and H cells, I_M and I_H, are generally smaller than biomass M and H , respectively. At the end of T, Adult communities are sorted according to their $P(T)$ values. The Adult community with the highest $P(T)$ (or a randomly-chosen Adult in control simulations) is selected for reproduction.

For community reproduction, we save the current random number generator state to be used to generate random numbers for partitioning the Adult. We partition Adult into Newborns of $\sim BM_{target}$ while allowing total biomass (total cell number) and $\phi_M(0)$ to fluctuate, such as occurring during pipetting. Specifically, the fold by which this Adult will be diluted is $n_D = \lfloor (M(T) + H(T))/BM_{target} \rfloor$ where $BM_{target} = 100$ is the pre-set target for Newborn total biomass, and $\lfloor x \rfloor$ is the floor function that generates the largest integer that is smaller than x. $I_H + I_M$ random integers between 1 and n_D are uniformly generated so that each M and H cell is assigned a random integer between 1 and n_D. All cells assigned with the same random integer belong to the same Newborn. This generates n_D newborn communities. This partition regimen can be experimentally implemented by pipetting $1/n_D$ volume of an Adult community into a new well. If n_D is less than n_{tot} (the total number of communities under selection), all n_D newborn communities are kept. Then, we partition the Adult with the next highest function (or a random community in control simulations) to obtain an additional batch of n_D Newborns until we obtain n_{tot} Newborns. The next cycle then begins.

To fix $BM(0)$ to BM_{target} and $\phi_M(0)$ to $\phi_M(T)$ of the parent Adult, the code randomly picks M cells from the selected Adult until the total biomass of M comes closest to $BM_{target}\phi_M(T)$ without exceeding it. H cells are sorted similarly. Because each M and H cells has a length between 1 and 2, the biomass of M can vary between $BM_{target}\phi_M(T) - 2$ and $BM_{target}\phi_M(T)$ and the biomass of H can vary between $BM_{target}(1-\phi_M(T)) - 2$ and $BM_{target}(1-\phi_M(T))$. Variations in $BM(0)$ and $\phi_M(0)$ are sufficiently small so that community selection improves $\overline{f}_P(T)$ (Figure 6 G and H). We have also performed simulations where the total number of cells is set to $\lfloor BM_{target}/1.5 \rfloor$ with $\lfloor BM_{target}\varphi_M(T)/1.5 \rfloor$ M cells and $\lfloor BM_{target}(1 - \varphi_M(T))/1.5 \rfloor$ H cells where $\varphi_M(T) = I_M(T)/(I_M(T) + I_H(T))$ is calculated

from the numbers instead of biomass of M and H cells. We obtain the same conclusion (Figure S25, right panels).

To fix Newborn total biomass $BM(0)$ to the target total biomass BM_{target} while allowing $\phi_M(0)$ to fluctuate (Figure 6 C and D), total biomass $BM(0)$ is counted so that $BM(0)$ comes closest to BM_{target} without exceeding it (otherwise, $P(T)$ may exceed the theoretical maximum). For example, suppose that a certain number of M and H cells have been sorted into a Newborn so that the total biomass is 98.6. If the next cell, either M or H, has a biomass of 1.3, this cell goes into the community so that the total biomass is $98.6 + 1.3 = 99.9$. However, if a cell of mass 1.6 happens to be picked, this cell doesn't go into this community so that this Newborn has a total biomass of 98.6 and the cell of mass 1.6 goes to the next Newborn. Thus, each Newborn may not have exactly the biomass of BM_{target} , but rather between $BM_{target} - 2$ and BM_{target}. Experimentally, total biomass can be determined from the optical density, or from the total fluorescence if cells are fluorescently labeled ([35]). To fix Newborn total cell number (instead of total biomass), the code sorts a total of $\lfloor BM_{target}/1.5 \rfloor$ cells into each Newborn, assuming that the average biomass of an M or H cell is 1.5. We obtain the same conclusion, as shown in Figure S25.

To fix $\phi_M(0)$ to $\phi_M(T)$ of the selected Adult community from the previous cycle while allowing $BM(0)$ to fluctuate (Figure 6 E and F), the code first calculates dilution fold n_D in the same fashion as mentioned above. $I_M(T)$ random integers between [1, n_D] are then generated for each M cell. All M cells assigned the same random integer belong to the same Newborn community. The code then randomly dispenses H cells into each Newborn until the total biomass of H comes closest to $M(0)(1 - \phi_M(T))/\phi_M(T)$ without exceeding it. Again, because each M and H has a biomass (or length) between 1 and 2, $\phi_M(0)$ of each Newborn community may not be exactly $\phi_M(T)$ of the selected Adult community. We have also performed simulations where the ratio of M and H cell numbers in the Newborn community, $I_M(0)/I_H(0)$, is set to $I_M(T)/I_H(T)$ of the Adult community, and obtain the same conclusion (Figure S25 center panels).

7 Problems associated with alternative definitions of community function and alternative means of reproducing an Adult

We describe problems associated with two alternative definitions of community function. Let's consider a simpler case where groups of Manufacturers are selected for high $P(T)$, and cell death is negligible. We have

$$\frac{dM}{dt} = (1 - f_P) g_M M$$

$$\frac{dP}{dt} = f_P g_M M$$

where biomass growth rate g_M is a function of B and R. Thus,

$$\frac{dM}{(1 - f_P)dt} = \frac{dP}{f_P dt}$$

and we have

$$P(T) = \frac{f_P}{1 - f_P} \left(M(T) - M(0)\right) \approx \frac{f_P}{1 - f_P} M(T)$$

if $M(T) \gg M(0)$ (true if T is long enough for cells to double at least three or four times).

If we define community function as $P(T)/M(T) \approx \frac{f_P}{1-f_P}$ (total Product normalized against *M* biomass in Adult community), then higher $\frac{f_P}{1-f_P}$ or higher f_P always leads to higher community function. Higher f_P in turn leads to *M* extinction (Figure 1).

If the community function is instead defined as $P(T)/M(0)$, then

$$\frac{P(T)}{M(0)} \approx \frac{f_P}{1-f_P}\frac{M(T)}{M(0)} = \frac{f_P}{1-f_P}\exp\left((1-f_P)\int_T g_M dt\right) \tag{27}$$

From Eq. 27, at a fixed f_P, $\frac{P(T)}{M(0)}$ increases as $\int_T g_M dt$ increases. $\int_T g_M dt$ increases as $\phi_M(0)$ decreases, since the larger fraction of Helper, the faster the accumulation of Byproduct and the larger $\int_T g_M dt$ (Figure S24B). Thus, we end up selecting communities with small $\phi_M(0)$ (Figure S6). This means that Manufactures could get lost during community reproduction, and community selection then fails.

If Resource is unlimited, then it will be problematic to reproduce an Adult by diluting it by a fixed-fold to Newborns. This is because with unlimited Resource, there is no competition between H and M. According to Eq. 27, $P(T)$ increases linearly with $M(0)$. $P(T)$ also increases with $H(0)$, since higher $H(0)$ leads to higher Byproduct and consequently higher $\int_T g_M dt$ in the exponent. Thus each cycle, communities with larger $BM(0)$ (instead of higher f_p) will get selected.

8 f_P^* is smaller for M group than for H-M community

For groups or communities with a certain $\int_T g_M dt$, we can calculate f_P optimal for community function from Eq. 27 by setting

$$\frac{dP(T)}{df_p} = M(0)\frac{d}{df_p}\left[\frac{f_P}{1-f_P}\exp\left((1-f_P)\int_T g_M dt\right)\right] = 0$$

We have

$$\frac{1}{(1-f_P)^2}\exp\left((1-f_P)\int_T g_M dt\right) - \frac{f_P}{1-f_P}\int_T g_M dt \exp\left((1-f_P)\int_T g_M dt\right) = 0$$

or

$$1/\int_T g_M dt = f_P(1-f_P).$$

If $\int_T g_M dt \gg 1$, f_P is very small, then the optimal f_P for $P(T)$ is

$$f_P^* \approx \left(\int_T g_M dt\right)^{-1} \tag{28}$$

M grows faster in monoculture than in community because B is supplied in excess in monoculture while in community, H-supplied Byproduct is initially limiting. Thus, $\int_T g_M dt$ is larger in monoculture than in community. According to Eq. 28, $f_P^* = 1/\int_T g_M dt$ is smaller for monoculture than for community.

9 Stochastic fluctuations during community reproduction

$BM(0)$ fluctuates in a Poissonian fashion with a standard deviation of $\sqrt{\mathrm{E}[BM(0)]}$, where "E" means the expected value.

$M(0)$ and $H(0)$ fluctuate independently with a standard deviation of $\sqrt{\mathrm{E}[M(0)]} = \sqrt{BM_{target}\phi_M(T)}$ and $\sqrt{\mathrm{E}[H(0)]} = \sqrt{BM_{target}(1-\phi_M(T))}$, respectively. Therefore, $M(0)/H(0)$ fluctuates with a variance of

$$\begin{aligned}\mathrm{Var}[M(0)/H(0)] &= \left(\frac{\mathrm{E}[M(0)]}{\mathrm{E}[H(0)]}\right)^2 \left[\frac{\mathrm{Var}[M(0)]}{(\mathrm{E}[M(0)])^2} - 2\frac{\mathrm{Cov}[M(0),\, H(0)]}{\mathrm{E}[M(0)]\mathrm{E}[H(0)]} + \frac{\mathrm{Var}[H(0)]}{(\mathrm{E}[H(0)])^2}\right] \\ &= \left(\frac{\phi_M(T)}{(1-\phi_M(T))}\right)^2 \left[\frac{1}{BM_{target}\phi_M(T)} + \frac{1}{BM_{target}(1-\phi_M(T))}\right]\end{aligned}$$

where "Cov" means covariance and "Var" means variance, and $\phi_M(T)$ is the fraction of M biomass in the Adult community from which Newborns are generated.

10 Mutualistic H-M community

In the mutualistic H-M community, Byproduct inhibits the growth of H. According to [94], the growth rate of *E. coli* decreases exponentially as the exogenously added acetate concentration increases. Thus, we only need to modify the growth of H by a factor of $\exp(-B/B_0)$ where B is the concentration of Byproduct and B_0 is the concentration of Byproduct at which H's growth rate is reduced by e^{-1}~0.37:

$$\frac{dH}{dt} = \exp\left(-\frac{B}{B_0}\right)\frac{g_{Hmax}R}{R+K_{HR}}H - \delta_H H$$

The larger B_0, the less inhibitory effect Byproduct has on H and when $B_0 \to +\infty$ Byproduct does not inhibit the growth of H. For simulations in Figure S30, $B_0 = 2K_{MB}$.

Acknowledgment

We thank the following for discussions: Lin Chao (UCSD), Maitreya Dunham (UW Seattle), Corina Tarnita (Princeton), Harmit Malik (Fred Hutch), and Alvaro Sanchez (Yale). Some of these discussions took place at the 2017 "Systems Biology and Molecular Economy of Microbial Communities" workshop at the International Centre for Theoretical Physics, Trieste, Italy and at the 2018 "Physical Principles Governing the Organization of Microbial Communities" workshop at the Aspen Center for Physics, Colorado, USA. We thank Alex Yuan, Chichun Chen, Bill Hazelton, Samuel Hart, David Skelding, Doug Jackson, and Kirill Korolev for feedback on the manuscript. This research was supported by the High Performance Computing Shared Resource of the Fred Hutch (P30 CA015704).

Supplementary Figures

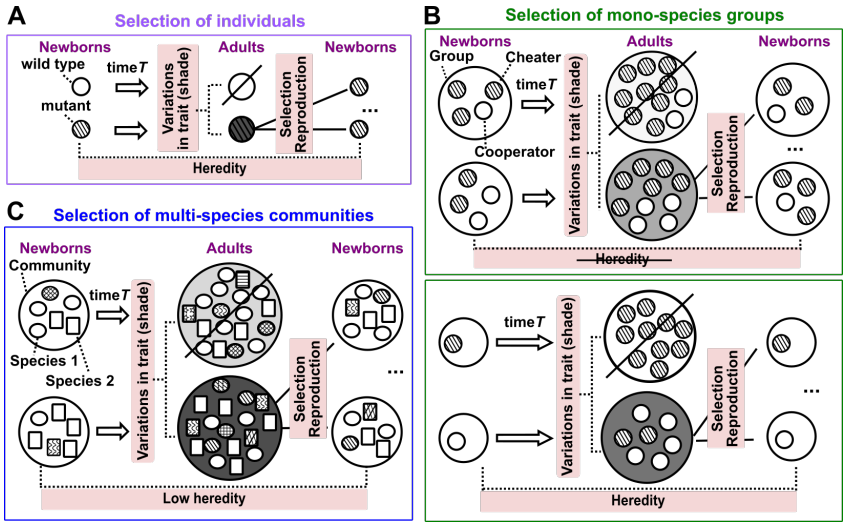

Figure S1: **Artificial selection is more challenging for multi-species communities than for individuals or mono-species groups.** Artificial selection can be applied to any population of entities [95]. An entity can be an individual (**A**), a mono-species group (**B**), or a multi-species community (**C**). Unlike natural selection which selects for fastest-growing cells, artificial selection generally selects for traits that are costly to individuals. In each selection cycle, a population of "Newborn" entities grow for maturation time T to become "Adults". Adults expressing a higher level of the trait of interest (darker shade) are selected to reproduce. An individual reproduces by making copies of itself, while an Adult group or community can reproduce by randomly splitting into multiple Newborns of the next selection cycle. Successful artificial selection requires that i) entities display trait variations; ii) trait variations can be selected to result in differential entity survival and reproduction; and iii) entity trait is sufficiently heritable from one selection cycle to the next [96]. In all three types of selection, entity variations can be introduced by mutations and recombinations in individuals. However, heredity can be low in community selection. (**A**) Artificial selection of individuals has been successful [97, 98, 99], since a trait is largely heritable so long as mutation and recombination are sufficiently rare. (**B, C**) In group and community selection, if T is small so that newly-arising genotypes cannot rise to high frequencies within a selection cycle, then Adult trait is mostly determined by Newborn *composition* (the biomass of each genotype in each member species). Then, *variation* can be defined as the dissimilarity in Newborn composition within a selection cycle, and *heredity* as the similarity of Newborn composition from one cycle to the next for Newborns connected through lineage (tubes with red outlines in Figure 3). (**B**) Artificial selection of mono-species groups has been successful [43, 45, 13]. Suppose cooperators but not cheaters pay a fitness cost to generate a product (shade). Artificial selection for groups producing high total product favors cooperator-dominated groups, although within a group, cheaters grow faster than cooperators. At a large Newborn population size (**top**), all Newborns will harbor similar fractions of cheaters, and thus inter-group variation will be small. During maturation, cheater frequency will increase, thereby diminishing heredity. In contrast, when Newborn groups are initiated at a small size such as one individual (**bottom**), a Newborn group will comprise either a cooperator or a cheater, thereby ensuring variation. Furthermore, even if cheaters were to arise during maturation, a fraction of Newborns of the next cycle will by chance inherit a cooperator, thereby ensuring some level of heredity. Thus, group selection can work when Newborn size is small. (**C**) Artificial selection of multi-species communities may be hindered by insufficient heredity. During maturation, the relative abundance of genotypes and species can rapidly change due to ecological interactions and evolution, which compromises heredity. During community reproduction, stochastic fluctuations in Newborn composition further reduce heredity.

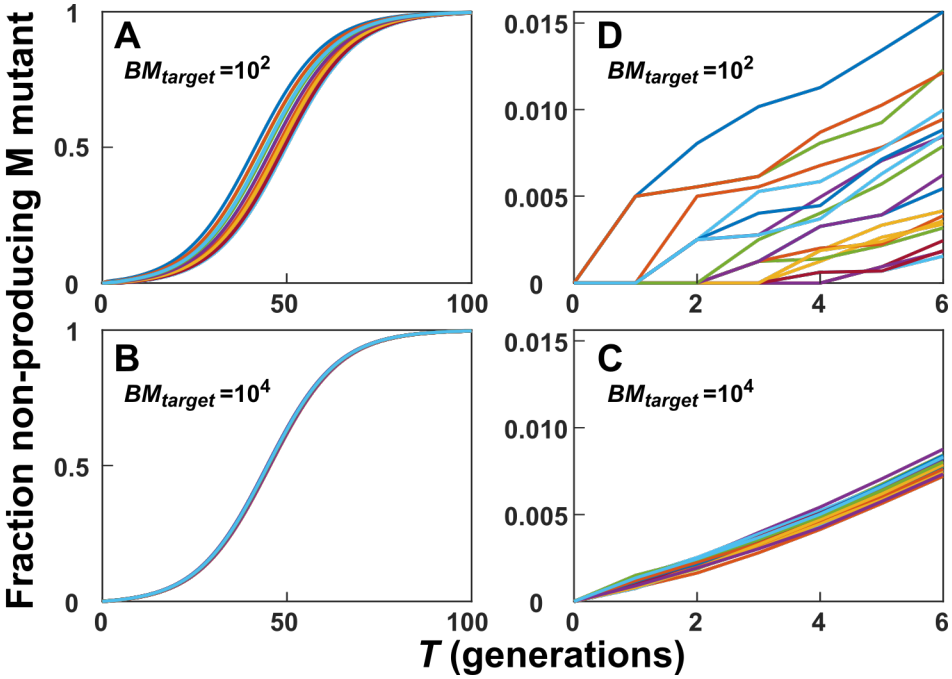

Figure S2: **Large Newborn size or long maturation time allows non-producers to accumulate and reduces inter-community variation.** From target total biomass of 10^2 or 10^4 wild-type cells, M population expands and mutates during a maturation time T that lasts 100 or 6 generations. Immediately following cell division, wild-type daughter cells mutate to non-producers with a probability of 10^{-3}. Wild-type and mutant cells follow exponential growth. The growth rate of wild-type cells is 0.87 that of mutants. The fraction of biomass made up by mutants at each wild-type doubling is shown. Note different scales. At 10^2 total biomass, a small fraction mutation (e.g. 0.005) means that some communities will remain free of non-producers at the end of T.

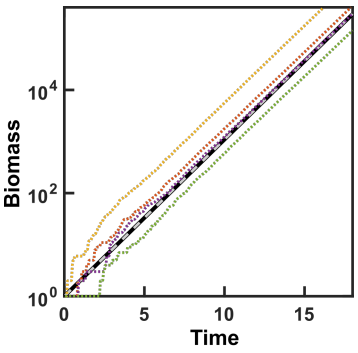

Figure S3: **A comparison of different growth models**. We model exponential biomass growth in excess metabolites. Thick black line: analytical solution with biomass growth rate (0.7/time unit). Grey dashed line: simulation assuming that biomass increases exponentially at 0.7/time unit and that cell division occurs upon reaching a biomass threshold, an assumption used in our model. Color dotted lines: simulations assuming that cell birth occurs at a probability equal to the birth rate multiplied with the length of simulation time step ($\Delta\tau = 0.05$ time unit). When a cell birth occurs, biomass increases discretely by 1, resulting in step-wise increase in color dotted lines at early time.

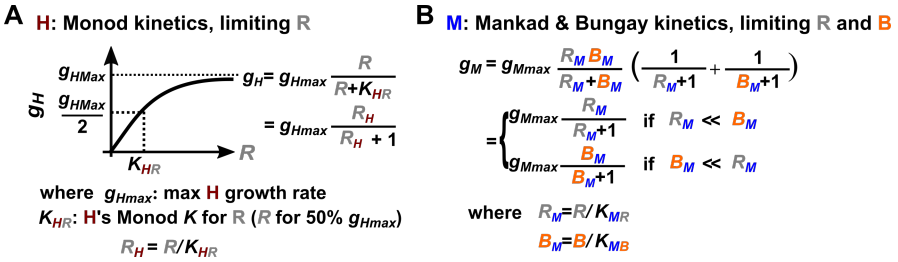

Figure S4: **Growth models of H and M.** (**A**) H growth follows Monod kinetics, reaching half maximal growth rate when $R = K_{HR}$. (**B**) M growth follows dual-substrate Mankad and Bungay kinetics. When Resource R is in great excess ($R_M \gg B_M$) or Byproduct B is in great excess ($B_M \gg R_M$), we recover mono-substrate Monod kinetics (**A**).

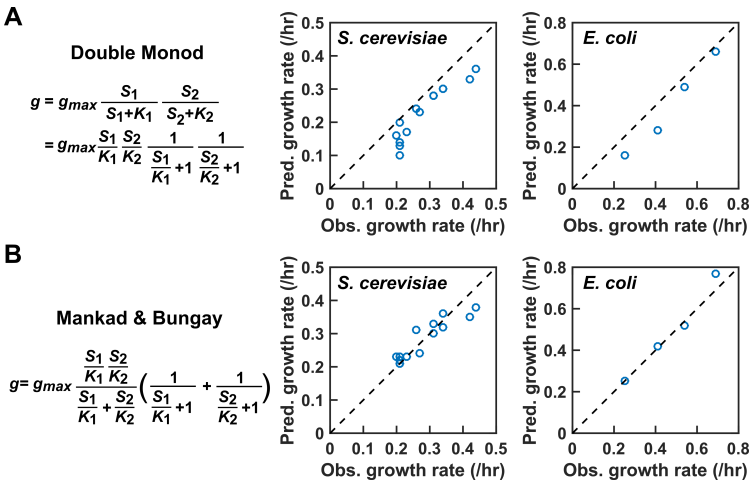

Figure S5: **A comparison of dual-substrate models.** Suppose that cell growth rate depends on each of the two substrates S_1 and S_2 in a Monod-like, saturable fashion. When S_2 is in excess, the S_1 at which half maximal growth rate is achieved is K_1. When S_1 is in excess, the S_2 at which half maximal growth rate is achieved is K_2. (**A**) In the "Double Monod" model, growth rate depends on the two limiting substrates in a multiplicative fashion. In the model proposed by Mankad and Bungay (**B**), growth rate takes a different form. In both models, when one substrate is in excess, growth rate depends on the other substrate in a Monod-fashion. However, when $\frac{S_1}{K_1} = \frac{S_2}{K_2} = 1$, the growth rate is predicted to be $g_{max}/2$ by Mankad & Bunday model, and $g_{max}/4$ by the Double Monod model. Mankad and Bungay model outperforms the Double Monod model in describing experimental data of *S. cerevisiae* and *E. coli* growing on low glucose and low nitrogen. The figures are plotted using data from Ref. [25].

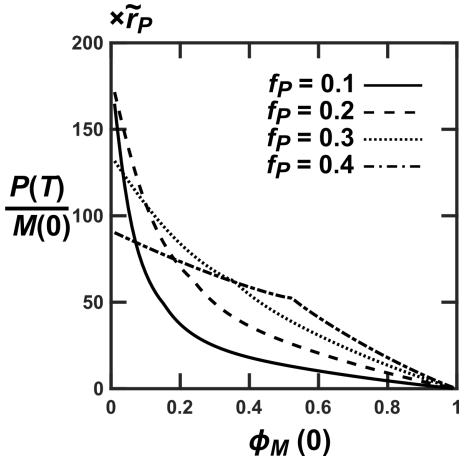

Figure S6: **Problems of defining community function as** $P(T)/M(0)$. Over the range of f_P where M and H can coexist, $P(T)/M(0)$ increases as $\phi_M(0)$ decreases. Thus, M can go extinct.

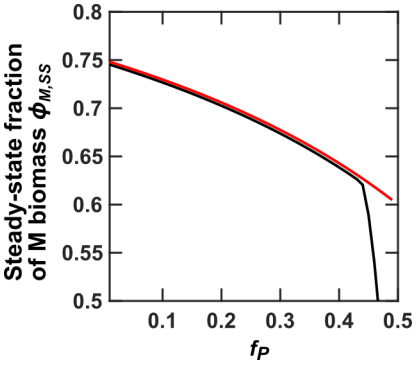

Figure S7: Comparison between the steady-state $\phi_{M,SS}$ calculated from Eqs. 6-10 (black curve) and from Eq. 14 (red line).

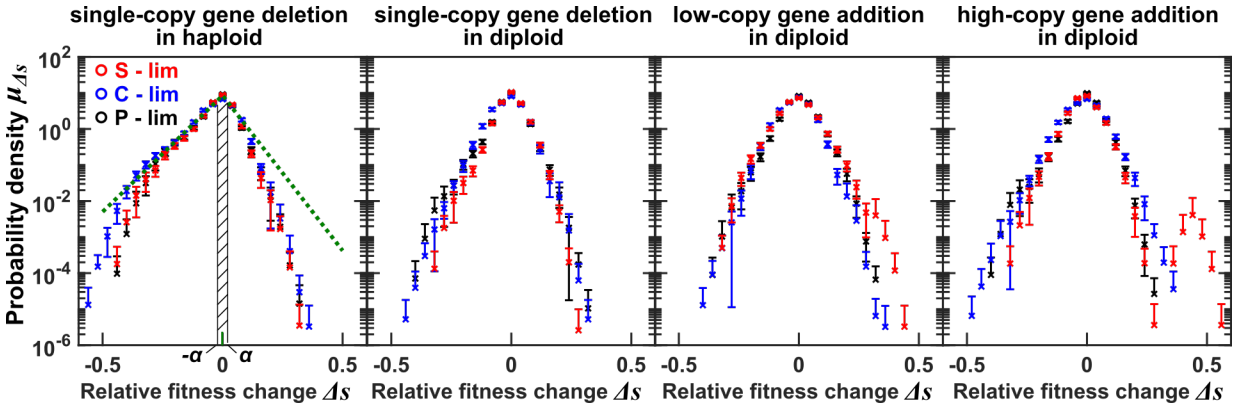

Figure S8: **Probability density functions of changes in relative fitness due to mutations ($\mu_{\Delta s}(\Delta s)$)**. We derived $\mu_{\Delta s}(\Delta s)$ from the Dunham lab data [34] where bar-coded mutant strains were competed under sulfate-limitation (red), carbon-limitation (blue), or phosphate-limitation (black). Error bars represent uncertainty $\delta\mu_{\Delta s}$ (the lower error bar is omitted if the lower estimate is negative). In the leftmost panel, green lines show non-linear least squared fitting of data to Eq. 19 using all three sets of data. Note that data with larger uncertainty are given less weight, and thus deviate more from the fitting lines. For an exponentially-distributed probability density function $p(x) = \exp(-x/r)/r$ where $x,\ r > 0$, the average of x is r. When plotted on a semi-log scale, we get a straight line with slope $1/r$, and inverting this gets us the average effect r. From the green line on the right side, we obtain the average effect of enhancing mutations $s_+ = 0.050 \pm 0.002$, and from the green line on the left side, we obtain the average effect of diminishing mutations $s_- = 0.067 \pm 0.003$. The probability of a mutation altering a phenotype by $\pm\alpha$ is the shaded area.

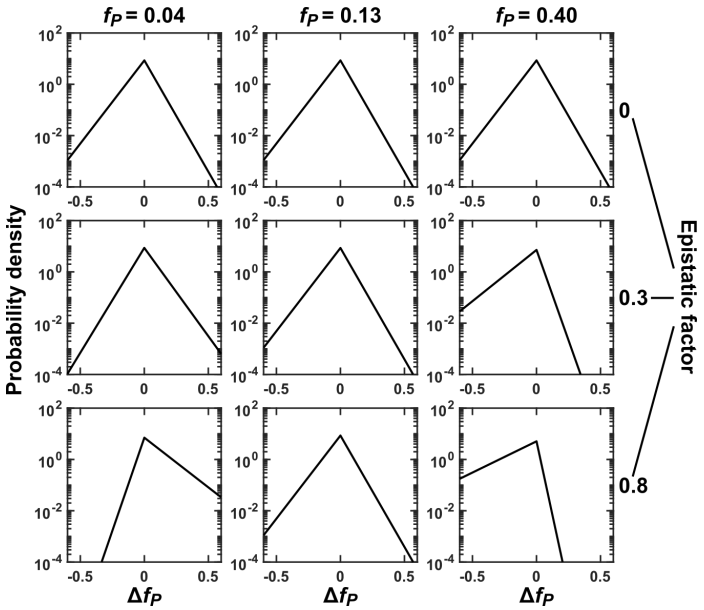

Figure S9: **Mutation effects under epistasis.** Distribution of mutation effects at different current f_P values (marked on top) are plotted. (Top) When there is no epistasis, distribution of mutational effects on f_P ($\triangle f_P$) are identical regardless of current f_P. (Middle and Bottom) With epistasis (see Methods Section 5 for definition of epistasis factor), mutational effects on f_P depend on the current value of f_P. If current f_P is low (left), enhancing mutations are more likely to occur (the area to the right of $\triangle f_P = 0$ becomes bigger) and their mean mutational effect becomes larger (mean=1/slope becomes larger due to smaller slope), while diminishing mutations are less likely to occur and their mean mutational effect is smaller. If current f_P is high (right), the opposite is true.

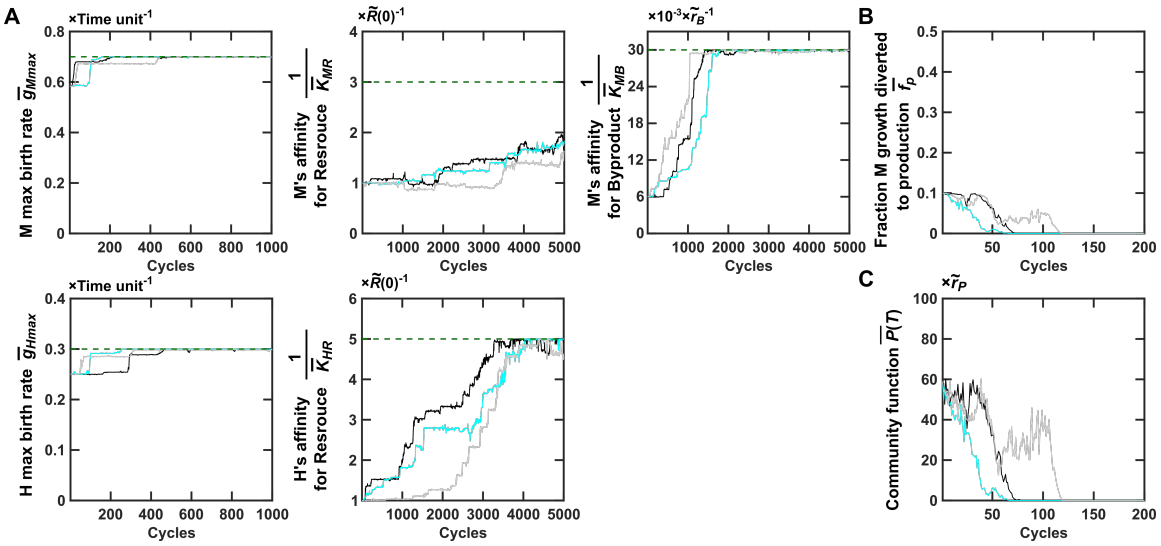

Figure S10: **Community function declines to zero in the absence of community selection**. Without community selection, natural selection favors fast growers with improved maximal growth rates and improved affinities for nutrients (**A**), and zero f_P (**B**). Consequently, $P(T)$ decreases to zero (**C**). Maximal growth rates of H and M (g_{Hmax} and g_{Mmax}), H's affinity for Resource $1/K_{HR}$, and M's affinity for Byproduct $1/K_{MB}$ rapidly improve to their respective upper bounds, while M's affinity for Resource $1/K_{MR}$ improves more slowly. This is consistent with M's growth being more limited by Byproduct. Green dashed lines: upper bounds of phenotypes; Magenta dashed lines: f_P optimal for community function and maximal $P(T)$ when all five growth parameters are fixed at their upper bounds and $\phi_M(0)$ is also optimal for $P(T)$. Black, cyan, and gray curves show three independent simulations. $\overline{P}(T)$ is averaged across selected Adults. $\bar{g}_{Mmax}$, $\bar{g}_{Hmax}$, and $\overline{f}_P$ are obtained by averaging within each selected Adult and then averaging across selected Adults. $K_{SpeciesMetabolite}$ are averaged within each selected Adult, then averaged across selected Adults, and finally inverted to represent average affinity. Note different x axis scales.

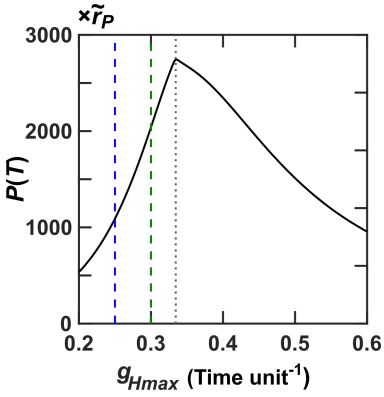

Figure S11: **Improving Helper g_{Hmax} does not necessarily improve community function**. We have chosen the ancestral (blue dashed line) and the biological upper bound (green dashed line) of g_{Hmax} such that improving g_{Hmax} improves community function. But suppose we have chosen ancestral g_{Hmax} at the grey dotted line, then higher g_{Hmax} would lower community function. The black solid curve is obtained by numerically integrating Eqs. 6-10 at different g_{Hmax} values where f_P is set to 0.4 and all growth parameters except for g_{Hmax} are set to their respective upper bounds. $BM(0)$ is 100, and $\phi_M(0)$ is 0.7 (close to steady-state value).

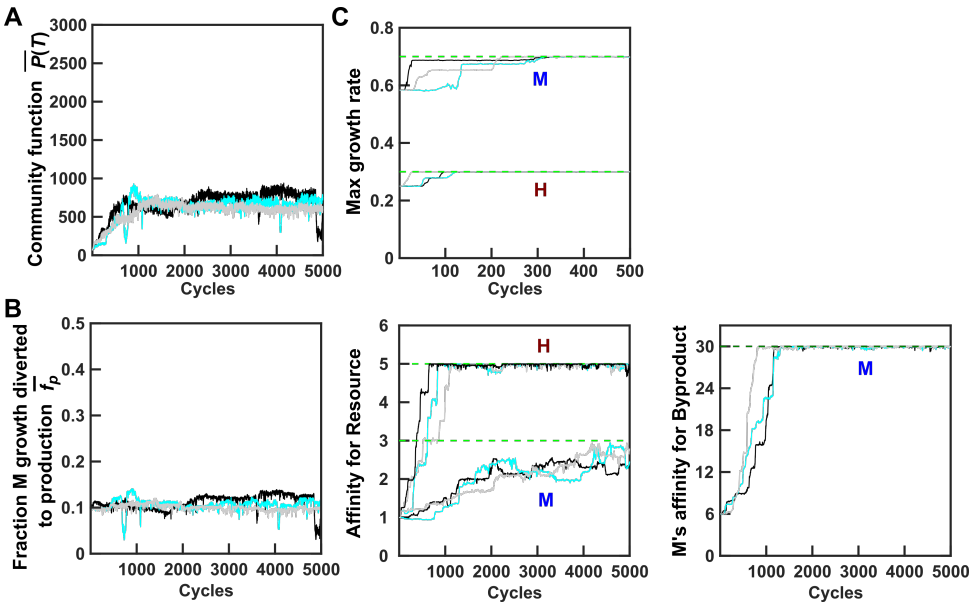

Figure S12: **Improved individual growth can promote community function.** Community function $P(T)$ increases upon community selection (**A**). Since f_P remains unchanged (**B**), this increase in $P(T)$ must be due to improved individual growth (**C**). Black, cyan, and gray curves show three independent simulation trials. Green dashed lines: upper bounds of the five growth parameters. The maximal growth rates (g_{Mmax} and g_{Hmax}) have the unit of 1/time. Affinity for Resource ($1/K_{MR}$, $1/K_{HR}$) has the unit of $1/\widetilde{R}(0)$, where $\widetilde{R}(0)$ is the initial amount of Resource in Newborn. Affinity for Byproduct ($1/K_{MB}$) has the unit of $1/\widetilde{r}_B$, where $\widetilde{r}_B$ is the amount of Byproduct released per H biomass produced. Product P has the unit of $\widetilde{r}_P$, the amount of Product released at the cost of one M biomass. More details can be found in Table 1. $\overline{P}(T)$ is averaged across selected Adults. $\bar{g}_{Mmax}$, $\bar{g}_{Hmax}$, and $\overline{f}_P$ are obtained by averaging within each selected Adult and then averaging across selected Adults. $K_{SpeciesMetabolite}$ are averaged within each selected Adult, then averaged across selected Adults, and finally inverted to represent average affinity.

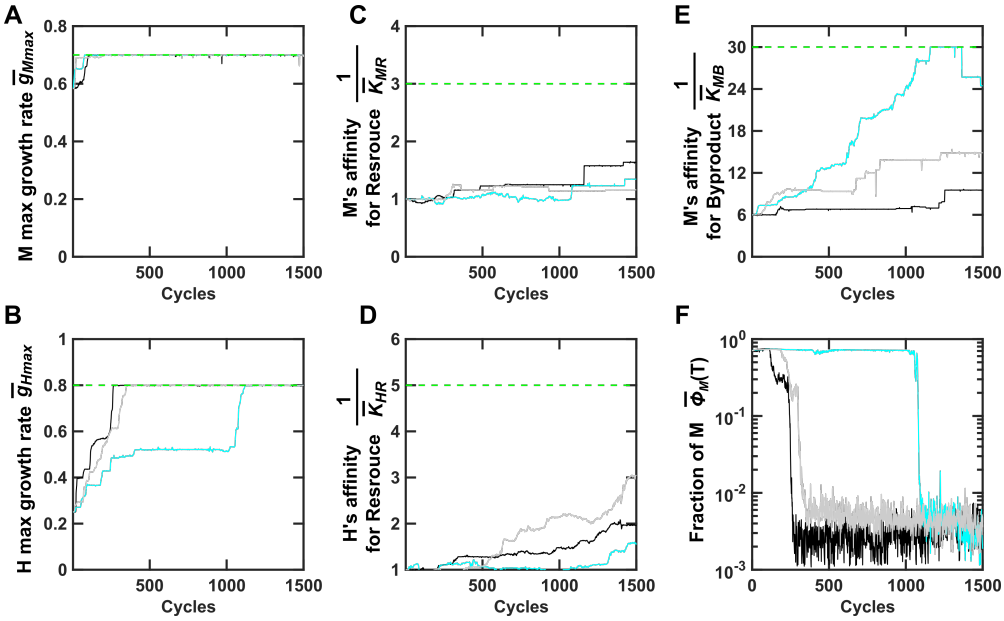

Figure S13: **Improving individual growth can impair community function.** (**A**-**E**) During community selection, growth parameters improved. Since the upper bound for g_{Hmax} ($g^*_{Hmax} = 0.8$) is larger than that of g_{Mmax} ($g^*_{Mmax} = 0.7$), natural selection eventually improved $g_{Hmax} > g_{Mmax}$. This would ordinarily lead to extinction of M. However, community selection managed to maintain M at a very low level (**F**). Black, cyan, and gray curves show three independent simulation trials. Green dashed lines: upper bounds of the five growth parameters. The maximal growth rates (g_{Mmax} and g_{Hmax}) have the unit of 1/time. Affinity for Resource ($1/K_{MR}$, $1/K_{HR}$) has the unit of $1/\widetilde{R}(0)$, where $\widetilde{R}(0)$ is the initial amount of Resource in Newborn. Affinity for Byproduct ($1/K_{MB}$) has the unit of $10^{-3}/\widetilde{r}_B$, where $\widetilde{r}_B$ is the amount of Byproduct released per H biomass produced. Product P has the unit of $\widetilde{r}_P$, the amount of Product released at the cost of one M biomass. $\overline{P}(T)$ is averaged across selected Adults. $\bar{g}_{Mmax}$, $\bar{g}_{Hmax}$, and $\overline{f}_P$ are obtained by averaging within each selected Adult and then averaging across selected Adults. $K_{SpeciesMetabolite}$ are averaged within each selected Adult, then averaged across selected Adults, and finally inverted to represent average affinity.

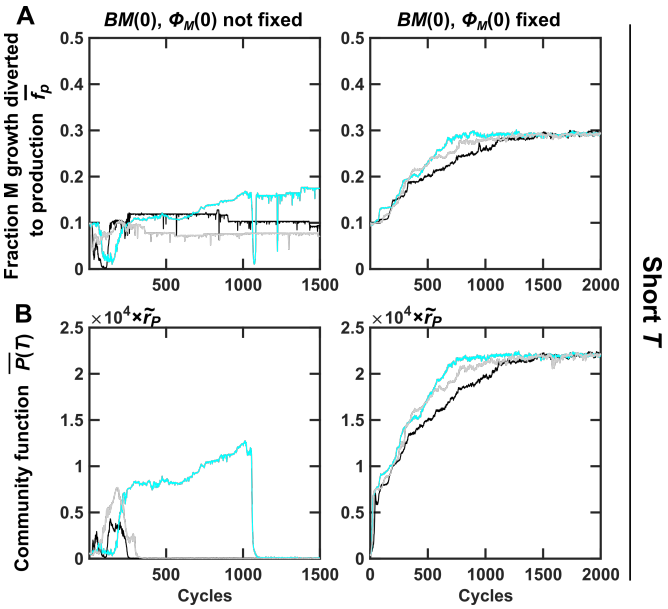

Figure S14: **Reducing non-heritable variations improves community function even when improved growth parameters impair community function.** Similar to Figure S13, the upper bound for g_{Hmax} ($g^*_{Hmax} = 0.8$) is larger than that of g_{Mmax} ($g^*_{Mmax} = 0.7$). When both $BM(0)$ and $\phi_M(0)$ were allowed to fluctuate stochastically, community function declined to very low levels due to low abundance of M (Figure S13F). Note that M did not go extinct because communities without any M would not be chosen to reproduce. When both $BM(0)$ and $\phi_M(0)$ were fixed, both $\overline{f}_P$ and $P(T)$ improved over cycles. Here, Resource supplied to Newborn communities could support 10^5 total biomass to accommodate faster growth rate.

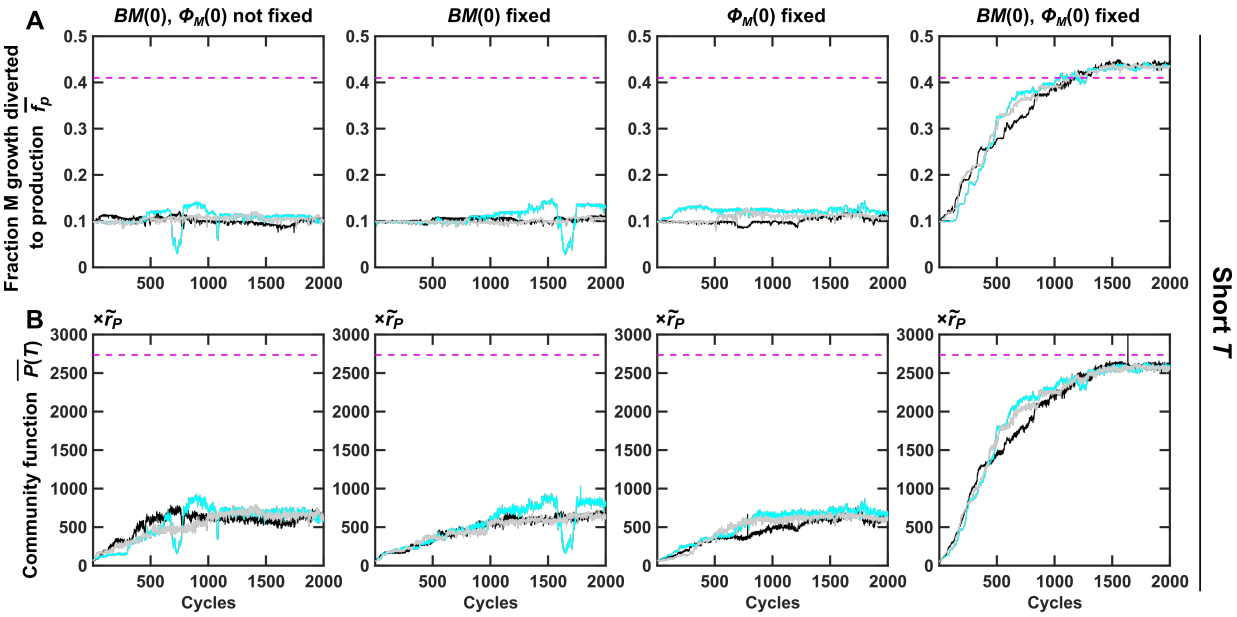

Figure S15: **Community selection succeeds when controlling the right experimental variables even if growth parameters are allowed to be modified by mutations.** Dynamics of (**A**) $\overline{f}_P(T)$ and (**B**) $\overline{P}(T)$ of selected communities when the maturation time $T = 17$, $g^*_{Hmax} = 0.3$ and $g^*_{Mmax} = 0.7$. All other simulation parameters are in Table 1. Compared to simulations whose results are presented in Figure 6, simulations for this figure allowed growth parameters of each M and H cells, and f_P of each M cell, to vary. The legends are the same as Figure 6.

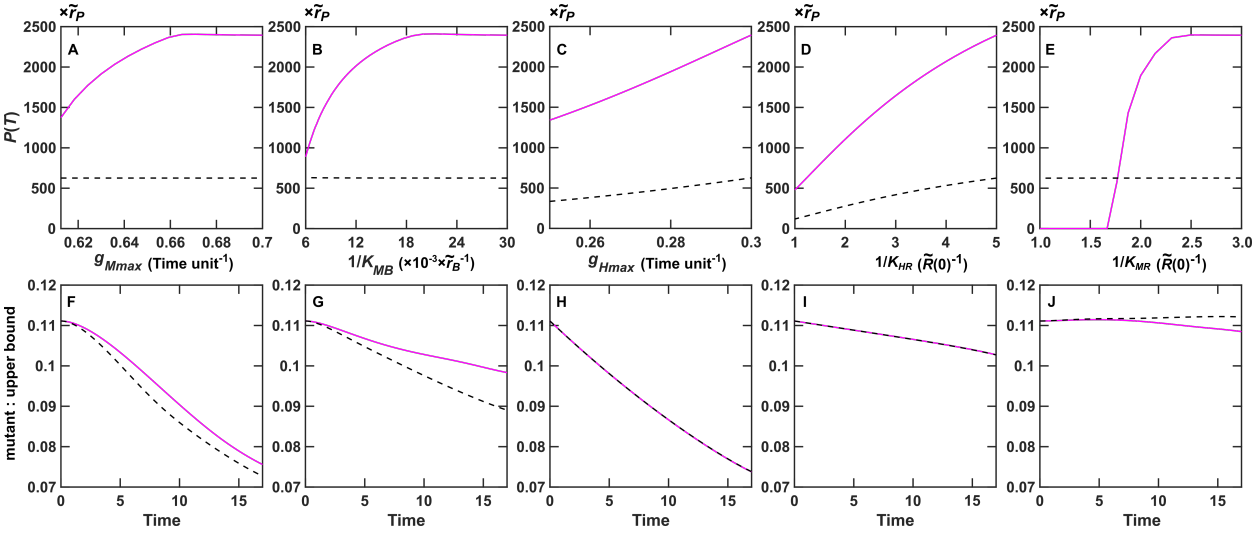

Figure S16: **Improving maximal growth rates and nutrient affinities generally, but do not always, improve individual fitness and community function.** In all figures, solid and dashed lines respectively represent dynamics when $f_P = f_P^* = 0.41$ (optimal for community function if all growth parameters are fixed at their upper bounds and $\phi_M(0) = 0.54$; Figure 5A) and $f_P = f_{P,Mono}^* = 0.13$ (optimal for M monoculture production when Byproduct is in excess; Figure 5B). (A-D) Community function increases as the indicated growth parameter increases (while all other growth parameters are fixed at upper bounds). For example, In (A), all growth parameters except for g_{Mmax} are at their upper bounds. For each g_{Mmax}, the steady-state $\phi_{M,SS}$ is calculated using equations in Methods Section 1. This steady-state $\phi_{M,SS}$ is then used to calculate $P(T)$. (F-I) respectively show that mutant individuals with the indicated growth parameter 10% lower than the upper bound have lower fitness. For example in (F), a Newborn community has 70 M and 30 H. 90% of M have upper bound $g_{Mmax} = 0.7$ ("upper bound"). 10% of M have $g_{Mmax} = 0.63$, 10% less than the upper bound ("mutant"). Other growth parameters are all at upper bounds. The ratio between mutant and upper bound drops over maturation time, indicating that M cells with mutant (lower) maximal growth rate have lower fitness. (E, J) When $f_P = 0.13$ (black dashed line) but not when $f_P = 0.41$ (magenta line), increasing M's affinity for Resource ($1/K_{MR}$) slightly decreases individual fitness, but this has only a slight effect on $P(T)$.

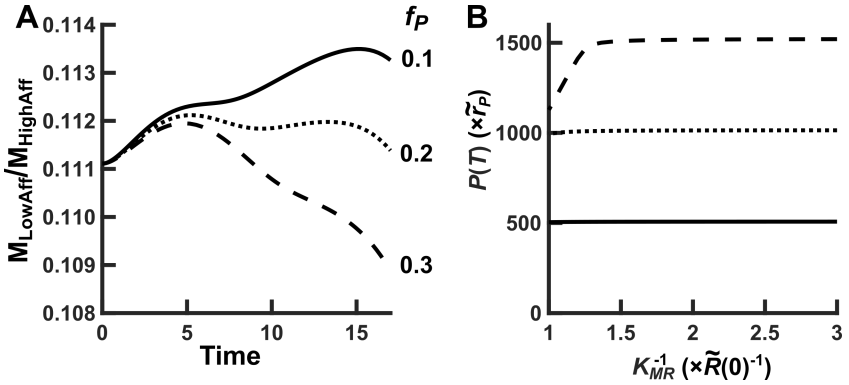

Figure S17: **At low f_P, M's lower affinity for Resource can increase its growth rate. (A)** The ratio between M_{LowAff} with low affinity for R ($K_{MR}^{-1} = 2.5\tilde{R}(0)^{-1}$) and $M_{HighAff}$ with high affinity for R ($K_{MR}^{-1} = 3\tilde{R}(0)^{-1}$) when their f_P is equal to 0.1 (solid line), 0.2 (dotted line) and 0.3 (dashed line) are plotted over one maturation cycle. **(B)** $P(T)$ improves over increasing affinity K_{MR}^{-1} when f_P is 0.1 (solid line), 0.2 (dotted line) and 0.3 (dashed line). The dependence of $P(T)$ on K_{MR}^{-1} is rather weak for low f_P. For example, when K_{MR}^{-1} increases from 1 to 3, $P(T)$ increases by only 2% and 0.6% for $f_P = 0.2$ and $f_P = 0.1$, respectively.

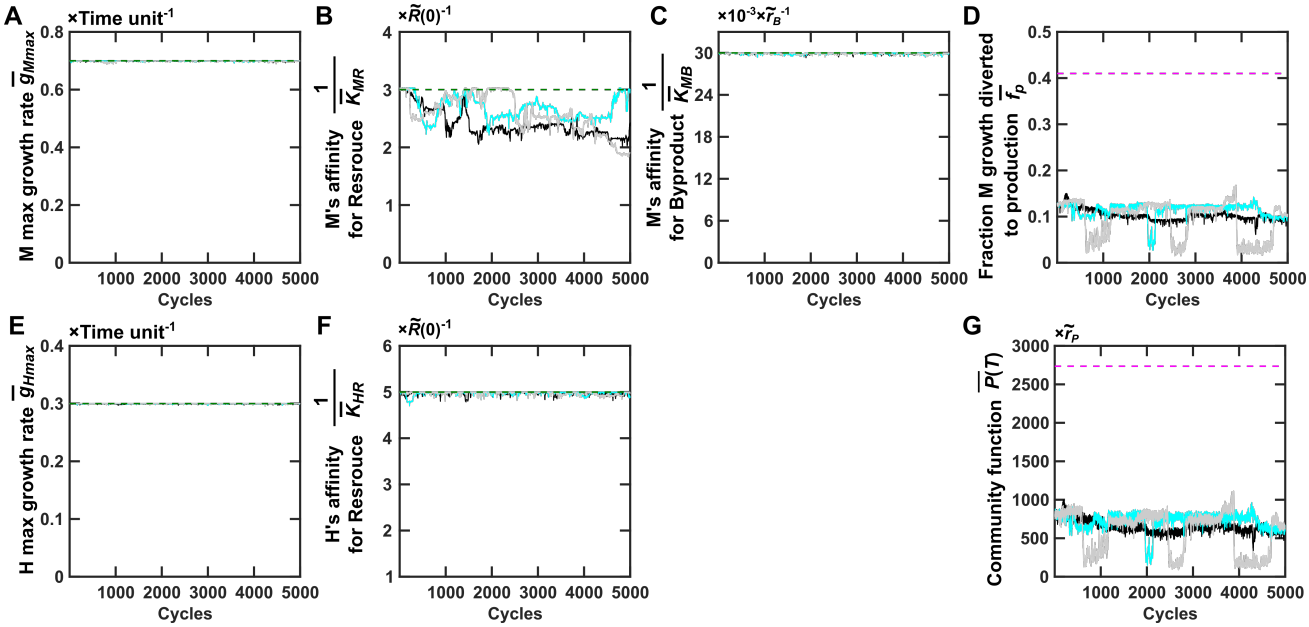

Figure S18: **Selection dynamics of communities of mono-adapted H and M when allowing all parameters to vary**. We start all growth parameters at their upper bounds and $f_P = f^*_{P,Mono} = 0.13$ (Figure 5B), and perform community selection while allowing all growth parameters and f_P to vary. M's affinity for R $1/\bar{K}_{MR}$ decreases slightly because at low $f_P = 0.13$, M with a lower affinity for R (lower $1/K_{MR}$) slightly improves individual fitness while slightly decreasing community function (Figure S17). Other growth parameters ($\bar{g}_{Mmax}$, $\bar{g}_{Hmax}$, $1/\bar{K}_{MB}$ and $1/\bar{K}_{HR}$) remain mostly constant during community selection because mutants with lower-than-maximal values are selected against by natural selection and by community selection (Figure S16). Other legend details can be found in Figure S10.

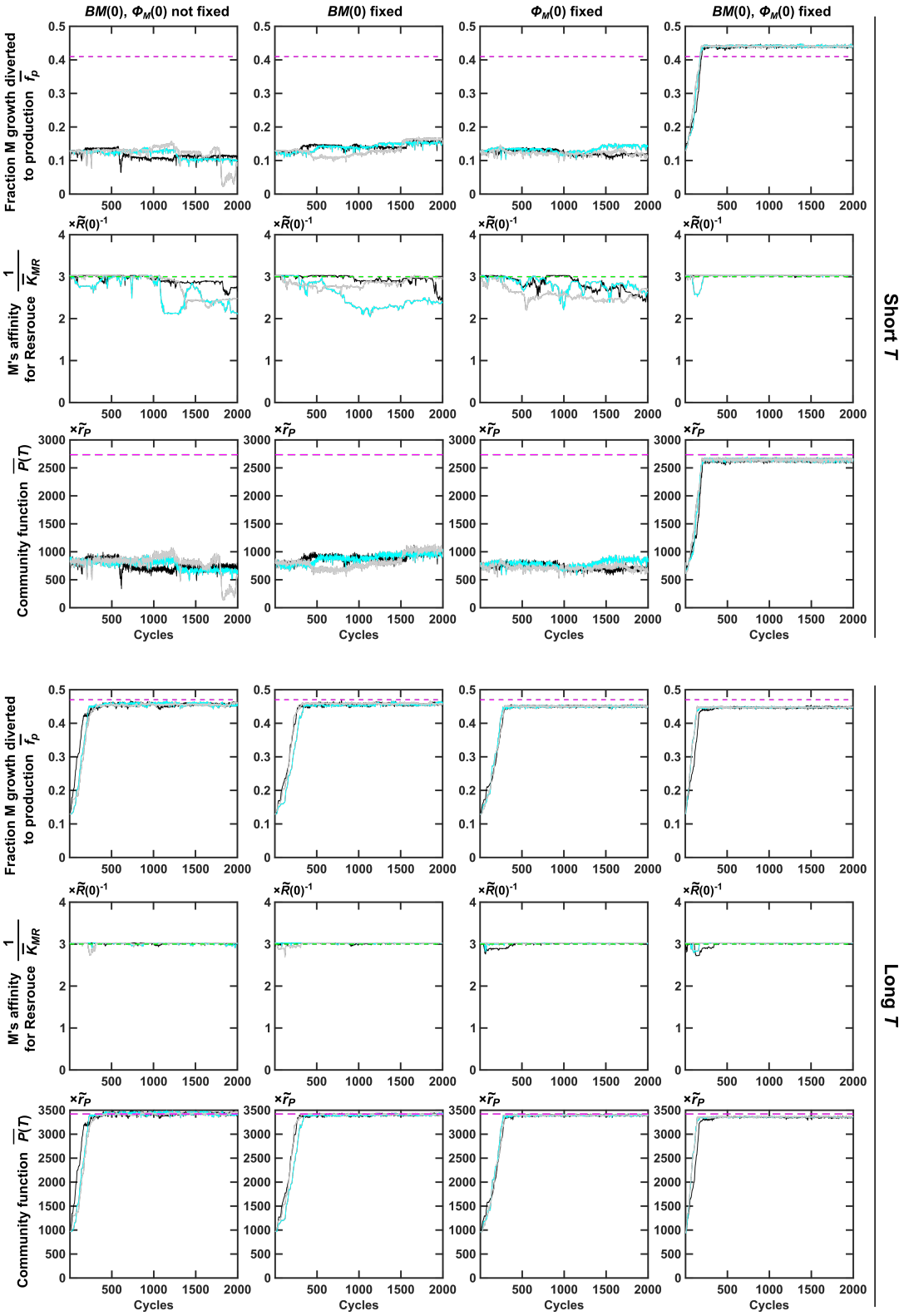

Figure S19: **Evolution dynamics of selected Adult communities when both f_P and K_{MR} are allowed to mutate.** The dynamics are similar to when only f_P is allowed to vary (Figure 6). Other legend details can be found in Figure S10.

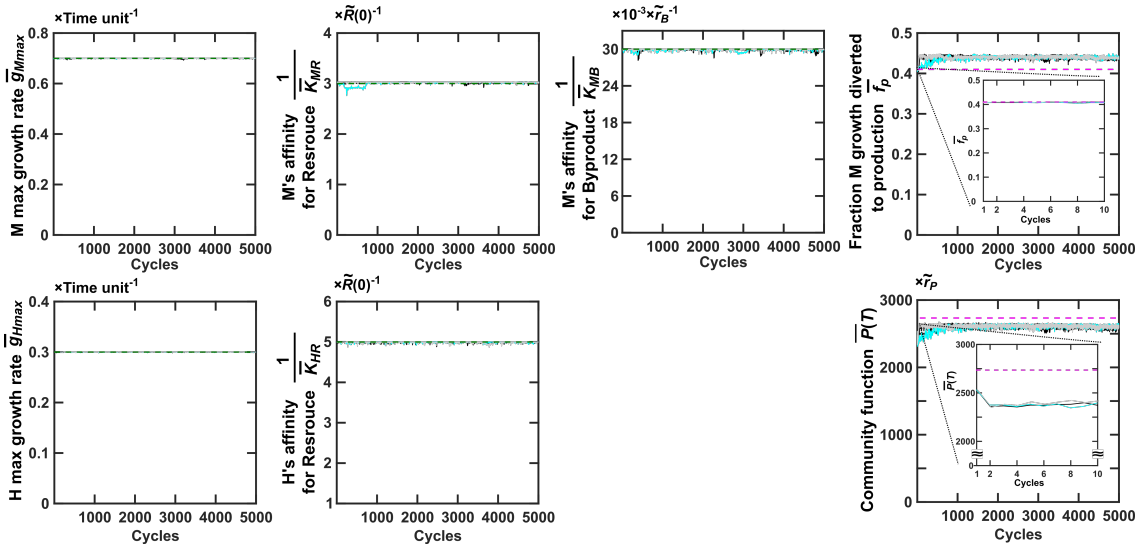

Figure S20: **Local optimality of community function $P^*(T)$.** We start each Newborn community with total biomass $BM(0)$=100, all five growth parameters at their upper bounds, and $f_P^* = 0.41$ and $\phi_M^*(0) = 0.54$ to achieve $P^*(T)$. We then allow all five growth parameters and f_P to mutate while applying community selection. To ensure effective community selection (Figure 6), $BM(0)$ is fixed to 100, and $\phi_M(0)$ is fixed to $\phi_M(T)$ of the previous cycle during community reproduction. We find that all five growth parameters remain at their respective evolutionary upper bounds. At the end of the first cycle (Cycle = 1 in insets), even though $\overline{f}_P$ has not changed, $\overline{P}(T)$ has already declined from the original magenta dashed line. This is because species interactions have driven $\phi_M(0)$ from the optimal $\phi_M^*(0)$ (=0.54) to near the steady state value (ϕ_M=0.73, compare with $\phi_{M,SS}$ represented by the green dashed line in Figure 1C bottom panel). Later, over hundreds of cycles, $\overline{f}_P$ gradually increases, which increases $\overline{P}(T)$. However, $\overline{P}(T)$ is still below maximal. This is because species composition gravitates toward steady state $\phi_{M,SS}$ which deviates from the optimal $\phi_M^*(0)$ ([60]). Other legend details can be found in Figure S10.

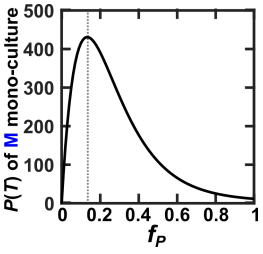

Figure S21: **Optimal f_P for accumulation of Product in an M monoculture is lower than that for an H-M community**. Suppose that a Newborn M group starts with a single Manufacturer (biomass 1) supplied with excess Byproduct and the same amount of Resource as in a Newborn H-M community. Then, maximal group function is achieved at a lower $f_P = f_{P,Mono}^* = 0.13$ ("mono-adapted", dashed line). Here, the growth parameters of M and H are all fixed at their upper bounds and $P(T)$ has the unit of $\widetilde{r}_P$.

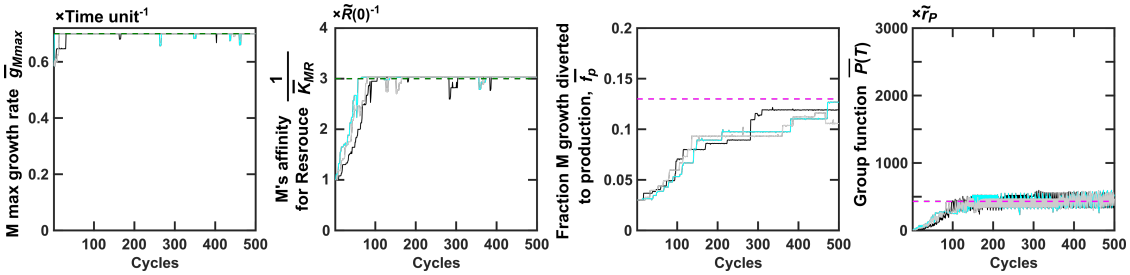

Figure S22: **Selection dynamics of M mono-species groups**. Phenotypes averaged over selected groups are plotted. Because Byproduct is in excess, K_{MB} terms are no longer relevant in equations (Figure S5, $R_M \ll B_M$). Upper bounds of g_{Mmax} and $1/K_{MR}$ are marked with green dashed lines. Magenta lines mark maximal f_P and $P(T)$ when g_{Mmax} and $1/K_{MR}$ are fixed at their upper bounds and when Byproduct is in excess.

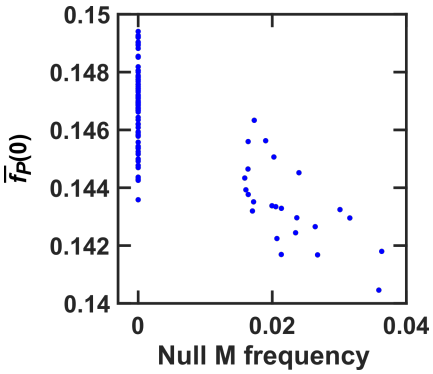

Figure S23: **The correlation between $\overline{f}_P(0)$ and the frequency of null M in a Newborn community.** As Newborns randomly sample M cells from the parent Adult community, their average $\overline{f}_P(0)$ partially correlates with the frequency of null M cells ($f_P = 0$).

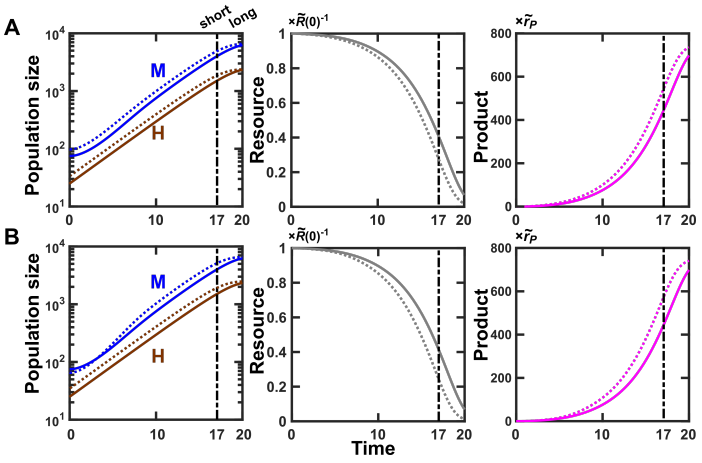

Figure S24: **Variations in community function can arise from non-heritable variations in Newborn compositions.** An average Newborn community (solid lines) has a total biomass of 100 with 75% M. (A) A "lucky" Newborn community (dotted lines), by stochastic fluctuations, has a total biomass of 130 with 75% M. Even though the two communities share identical $f_P = 0.1$, the Newborn with 130 total biomass has its M growing to a larger size (left), depleting more Resource (middle), and making more Product (right) by the end of short T (=17). (B) A "lucky" Newborn community (dotted lines), by stochastic fluctuations, has 100 total biomass with 65% M. Even though the two communities share identical $f_P = 0.1$, the Newborn with lower $\phi_M(0)$ (dotted) has its M enjoying a shorter growth lag and growing to a larger size (left), depleting more Resource (middle), and making more Product (right) by the end of short T (=17). In both cases, the difference between lucky (dotted) and average (solid) communities is diminished at longer T ($T = 20$) compared to shorter T ($T = 17$, dash dot line).

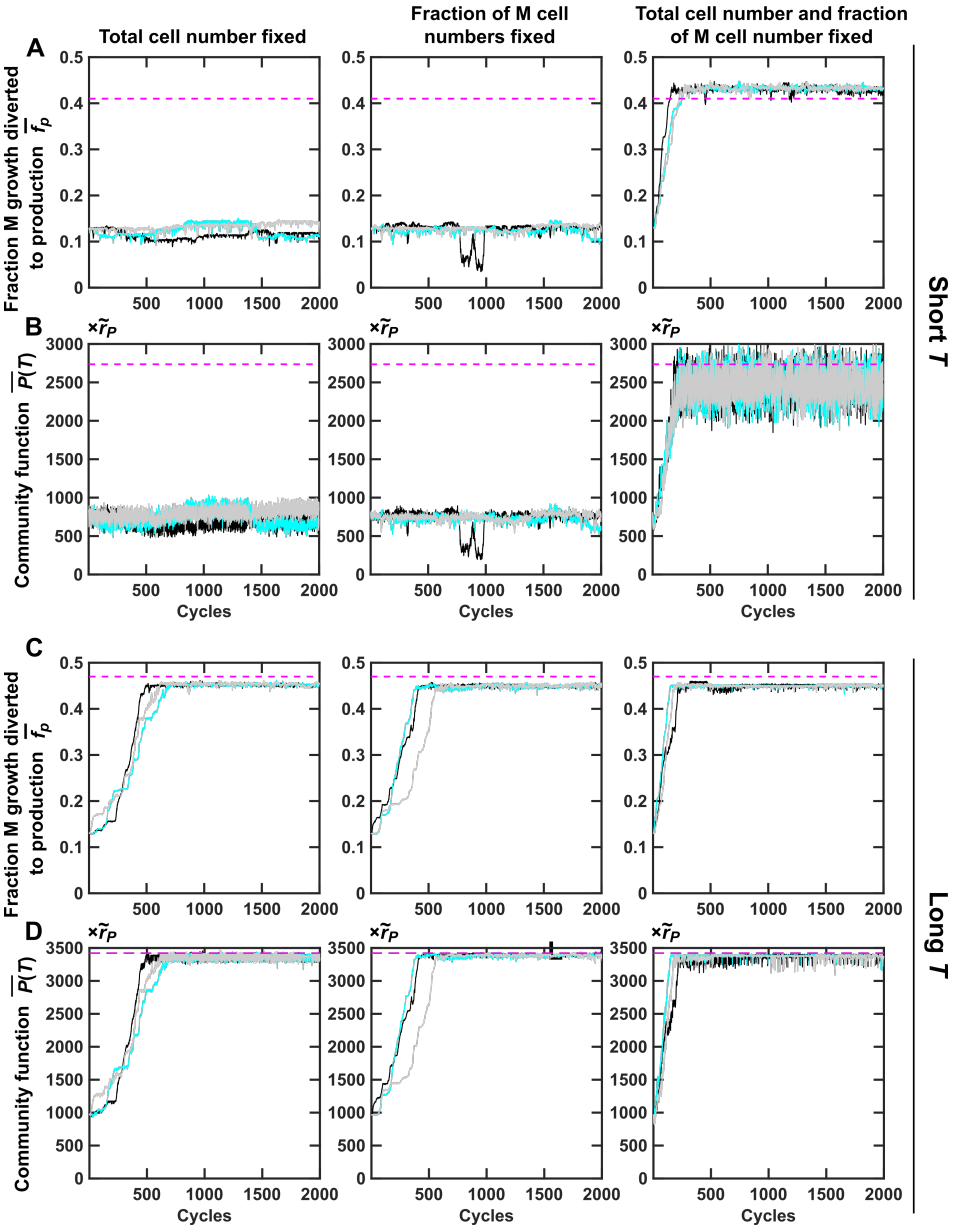

Figure S25: **Fixing H and M cell numbers (instead of biomass) during community reproduction allows short-T selection regimen to improve community function.** For left panels, the total cell number is fixed to $\lfloor N_0/1.5 \rfloor$ where $\lfloor x \rfloor$ means the largest integer without exceeding x. For center panels, the ratio between M and H cell numbers are fixed to $I_M(T)/I_H(T)$, where $I_M(T)$ and $I_H(T)$ are the number of M and H cells in the selected Adult community, respectively. For right panels, the total cell numbers are fixed to $\lfloor N_0/1.5 \rfloor$ and the ratio between M and H cell numbers are fixed to $I_M(T)/I_H(T)$. See Methods Section 6 for details of simulating community reproduction. Other legend details can be found in Figure 6.

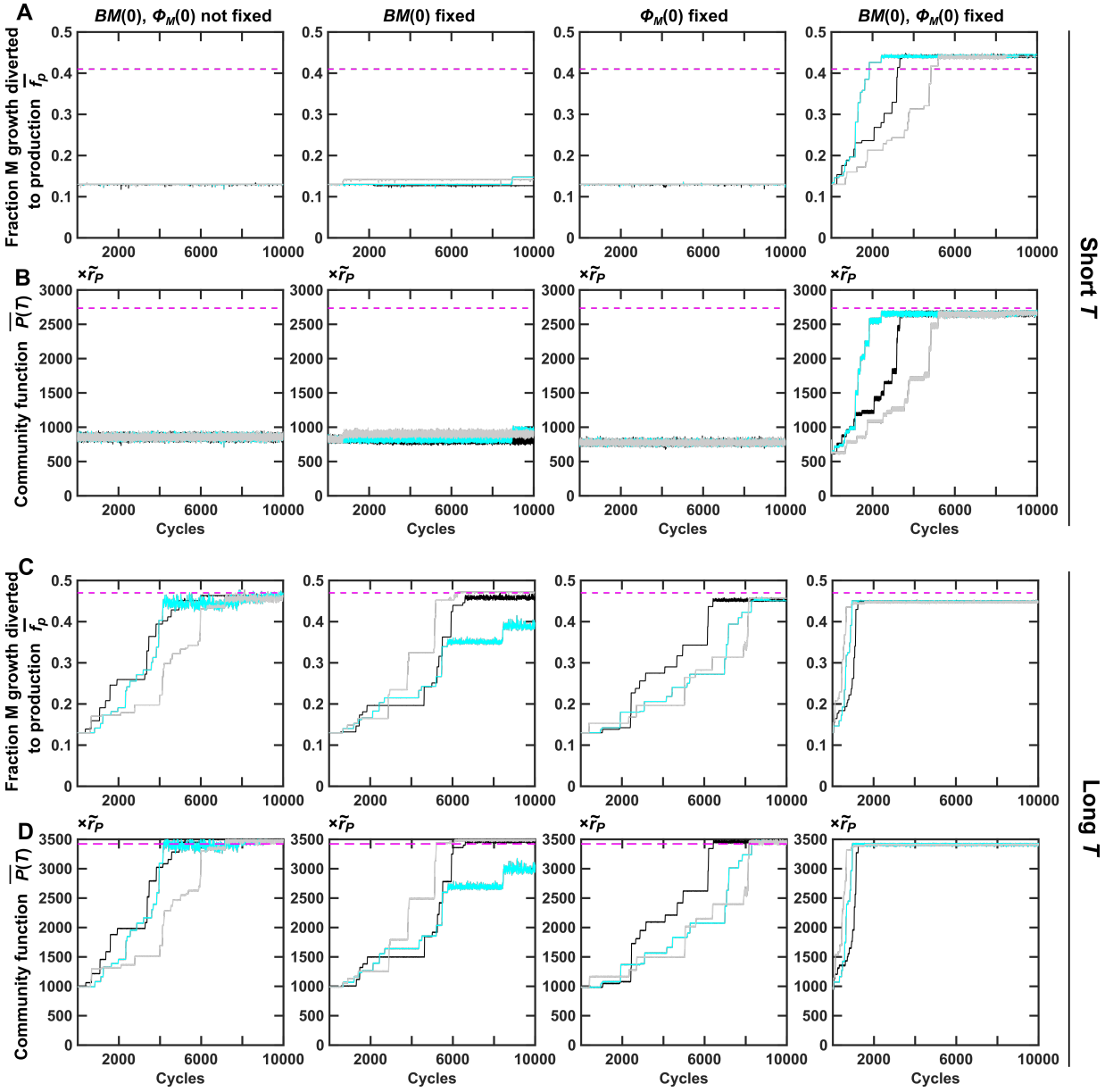

Figure S26: **Evolution dynamics of selected Adult communities at a mutation rate of 2×10^{-5} per cell per generation.** (**A, B**) At short maturation time ($T = 17$, Resource is not exhausted in an average community), fixing both $BM(0)$ and $\phi_M(0)$ is required for community function to improve. (**C, D**) At long maturation time ($T = 20$, Resource is nearly exhausted in an average community), community function improves without needing to fix $BM(0)$ or $\phi_M(0)$. When both are fixed, community function improves even faster. At this mutation rate, because the population size of a community never exceeds 10^4, a mutation occurs on average every 5 cycles, resulting in step-wise improvement in both $\overline{f}_P(T)$ and $\overline{P}(T)$. Other legend details can be found in Figure 6.

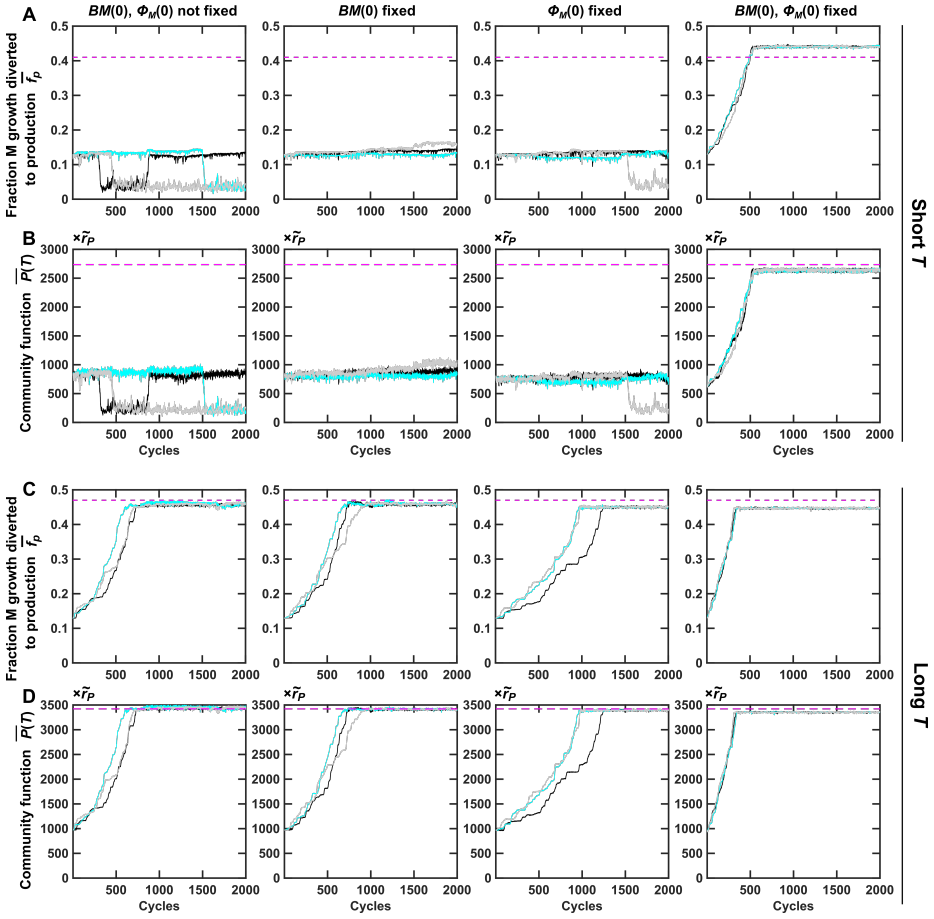

Figure S27: **Evolutionary dynamics of selected Adult communities under a different distribution of mutation effects.** Here, the distribution of mutation effects is specified by Eq. 19 where $s_+ = s_- = 0.02$ are constants. Other legend details can be found in Figure 6.

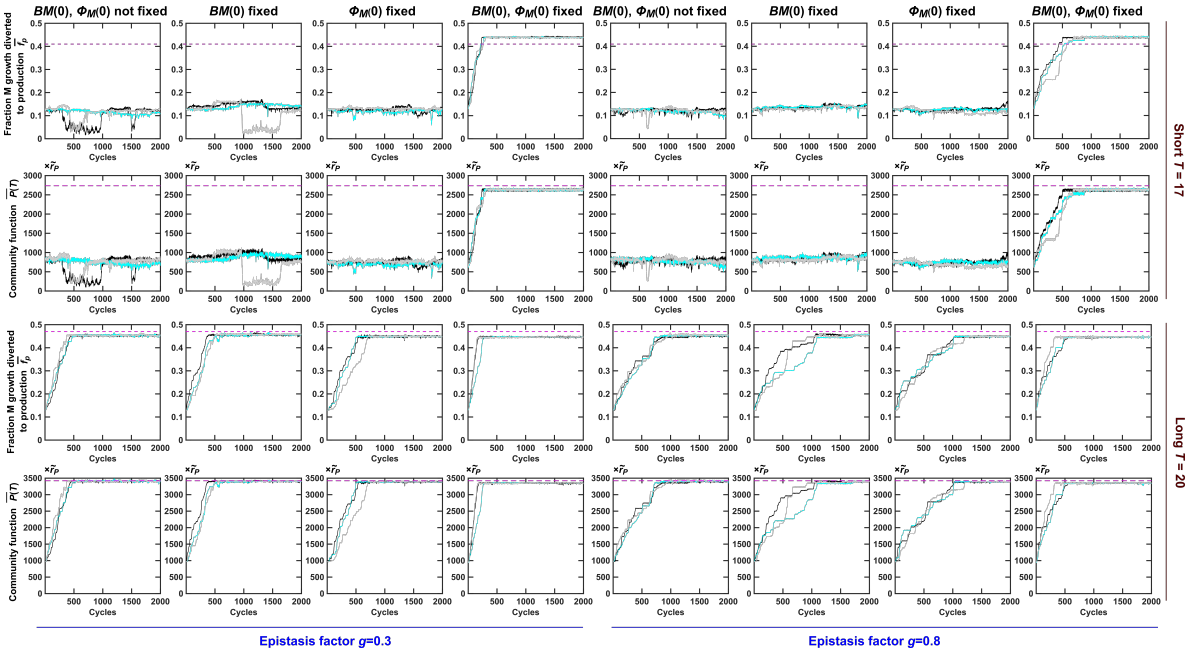

Figure S28: **Evolutionary dynamics of selected Adults when epistasis is considered.** When we incorporate different epistasis strengths (epistasis factor of 0.3 and 0.8), we obtain essentially the same conclusions as when epistasis is not considered (Figure 6). Other legend details can be found in Figure 6.

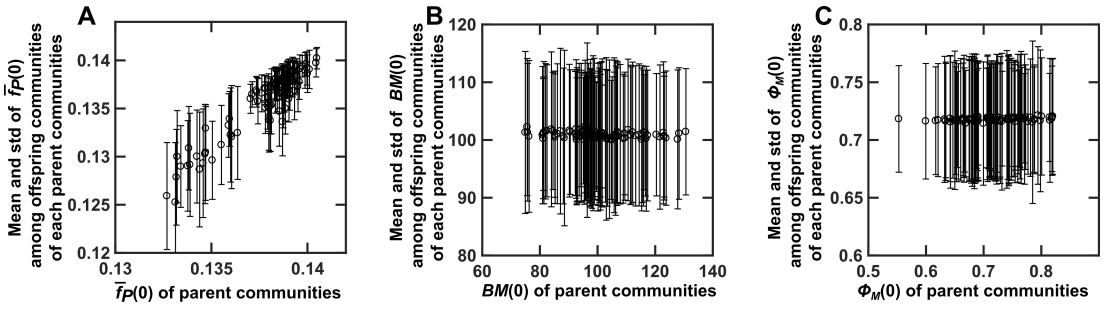

Figure S29: **Correlation of the three determinants of the community function between parent communities and offspring communities.** The scatter plots show the correlation between the offspring communities' determinants and their parent community's determinants. For example, the abscissa of each point in (**A**) indicates $\overline{f}_P(0)$ of a parent community; the ordinate and error bar of each point in (**A**) indicate the mean and standard deviation of $\overline{f}_P(0)$ among the offspring communities formed out of the parent community. 100 communities from the 100th cycle of one of the simulations shown in Figure 6A and B are analyzed to generate this plot.

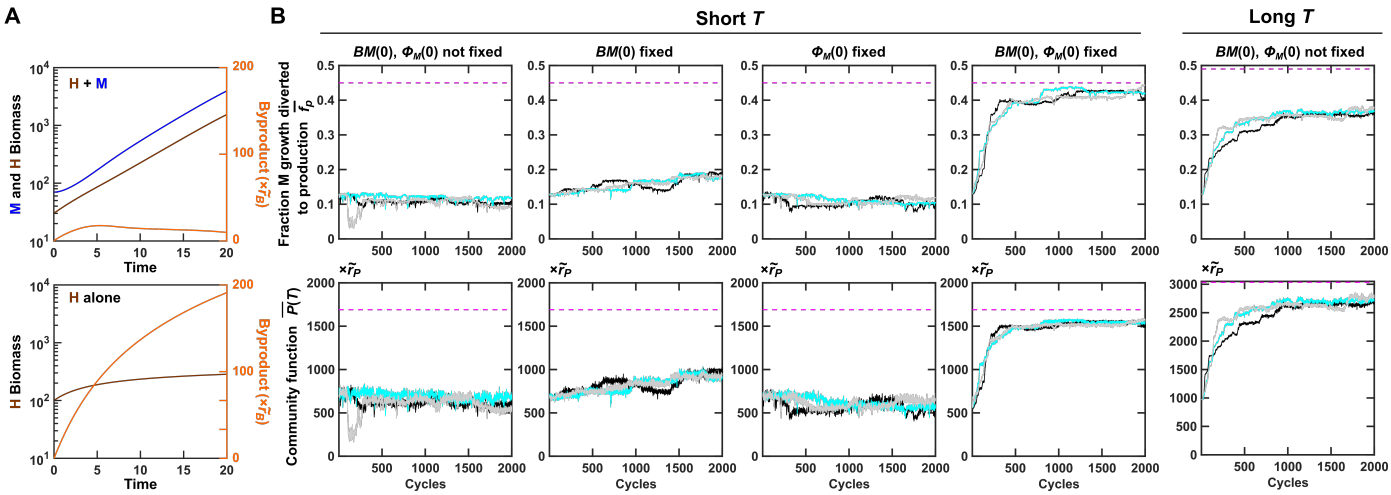

Figure S30: **Selection dynamics of mutualistic H-M communities.** In the mutualistic H-M community, H generates Byproduct which is essential for M but inhibitory to H. (**A**) H can grow to a high density in the presence of M (top) but not in the absence of M (bottom). (**B**) Similar to the commensal H-M community, selection works when non-heritable variations in $P(T)$ are suppressed either via fixing both $BM(0)$ and $\phi_M(0)$ at short T (=17) or via extending T (=20). Other legend details can be found in Figure 6.

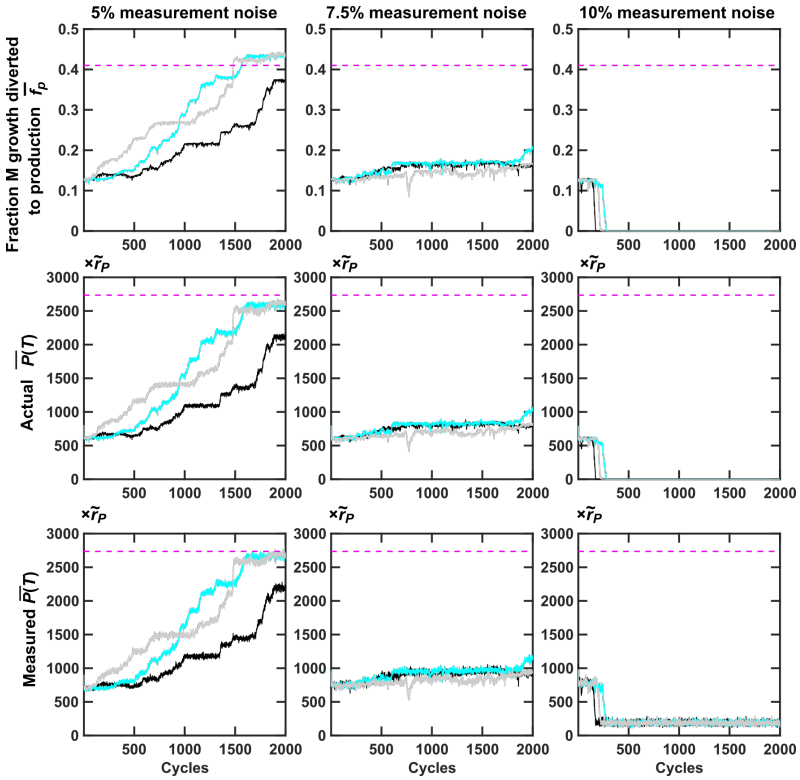

Figure S31: **Selection dynamics in the presence of measurement uncertainty in $P(T)$.** Evolution of $\overline{f}_P(T)$ and $\overline{P}(T)$ when Adult communities are chosen to reproduce based on "measured $P(T)$" - the sum of actual $P(T)$ and an "uncertainty term" randomly drawn from a normal distribution with zero mean. The amplitude of the noise is characterized by the standard deviation of the normal distribution. In the left, center, and right panels, the noise terms were drawn from normal distributions with standard deviations of 5%, 7.5%, and 10% of the ancestral $P(T)$, respectively. The middle and lower panels show the average actual $P(T)$ and the average measured $P(T)$, respectively.

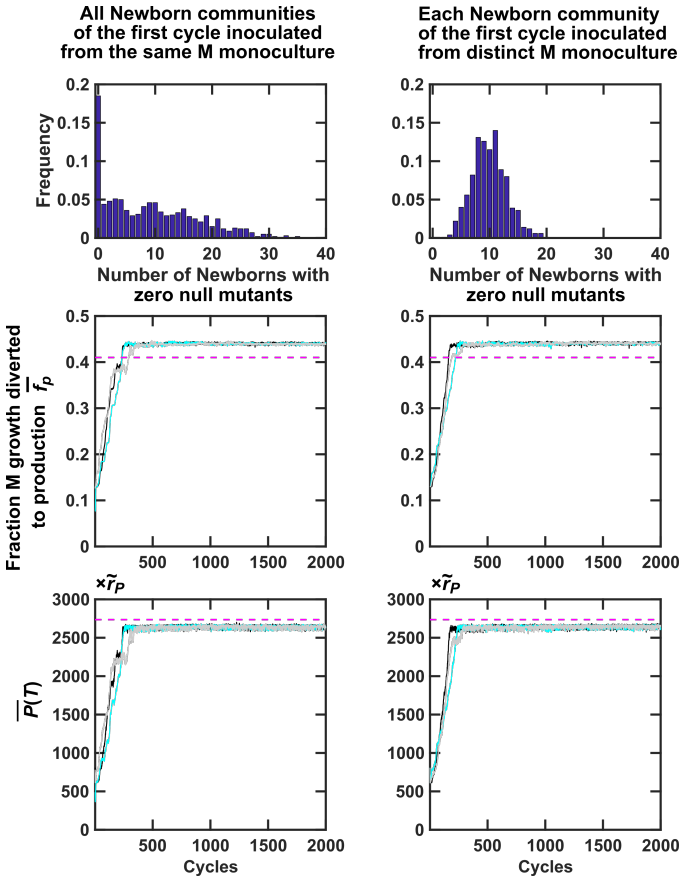

Figure S32: **Different ways of inoculating the Newborn communities of the first cycle had limited impact on selection dynamics.** (**Top Panel**) The number of communities initially free of non-producer M mutants depends on whether each Newborn community from the first cycle is inoculated from a distinct M monoculture. Each Newborn community for the first selection cycle was then inoculated with 60 M cells, either from the same M monoculture (**Left panel**), or from distinct M monocultures (**Right panel**). This pre-growth process is repeated 100 times, and the frequency of total numbers of Newborn communities out of 100 without non-producers is plotted. Selection dynamics are almost the same when the Newborn communities from the first cycle are inoculated by (**Left panel**) the same M monoculture or by (**Right panel**) distinct monocultures. Here we assumed that each monoculture grew from a single non-null M cell. This M cell went through ~23 doublings and therefore multiplied into $\sim 10^7$ cells. Every time a non-null M cell divides the mother and daughter cells can independently mutate and become a null M cell with $f_P = 0$ at a fixed probability of 10^{-3}. Assuming that all non-null M cells have identical $f_P = 0.13$, non-null M cells grow at a rate 87% of that of a null cell. As a result, after ~23 doublings, the M monocultures have on average ~3% null mutants.

References

[1] Trevor D. Lawley, Simon Clare, Alan W. Walker, Mark D. Stares, Thomas R. Connor, Claire Raisen, David Goulding, Roland Rad, Fernanda Schreiber, Cordelia Brandt, Laura J. Deakin, Derek J. Pickard, Sylvia H. Duncan, Harry J. Flint, Taane G. Clark, Julian Parkhill, and Gordon Dougan. Targeted restoration of the intestinal microbiota with a simple, defined bacteriotherapy resolves relapsing Clostridium difficile disease in mice. *PLoS pathogens*, 8(10):e1002995, 2012.

[2] Stefanie Widder, Rosalind J. Allen, Thomas Pfeiffer, Thomas P. Curtis, Carsten Wiuf, William T. Sloan, Otto X. Cordero, Sam P. Brown, Babak Momeni, Wenying Shou, Helen Kettle, Harry J. Flint, Andreas F. Haas, Béatrice Laroche, Jan-Ulrich Kreft, Paul B. Rainey, Shiri Freilich, Stefan Schuster, Kim Milferstedt, Jan R. van der Meer, Tobias Groβkopf, Jef Huisman, Andrew Free, Cristian Picioreanu, Christopher Quince, Isaac Klapper, Simon Labarthe, Barth F. Smets, Harris Wang, Isaac Newton Institute Fellows, and Orkun S. Soyer. Challenges in microbial ecology: building predictive understanding of community function and dynamics. *The ISME Journal*, March 2016. 00001.

[3] Stephen R. Lindemann, Hans C. Bernstein, Hyun-Seob Song, Jim K. Fredrickson, Matthew W. Fields, Wenying Shou, David R. Johnson, and Alexander S. Beliaev. Engineering microbial consortia for controllable outputs. *The ISME Journal*, 10(9):2077–2084, September 2016.

[4] Jian Zhou, Qian Ma, Hong Yi, Lili Wang, Hao Song, and Ying-Jin Yuan. Metabolome profiling reveals metabolic cooperation between Bacillus megaterium and Ketogulonicigenium vulgare during induced swarm motility. *Applied and Environmental Microbiology*, 77(19):7023–7030, October 2011. 00038.

[5] R. E. Wheatley. The consequences of volatile organic compound mediated bacterial and fungal interactions. *Antonie van Leeuwenhoek*, 81(1-4):357–364, December 2002. 00123.

[6] Kwang-sun Kim, Soohyun Lee, and Choong-Min Ryu. Interspecific bacterial sensing through airborne signals modulates locomotion and drug resistance. *Nature Communications*, 4:1809, 2013.

[7] Matthew F Traxler, Jeramie D Watrous, Theodore Alexandrov, Pieter C Dorrestein, and Roberto Kolter. Interspecies interactions stimulate diversification of the Streptomyces coelicolor secreted metabolome. *mBio*, 4(4), 2013.

[8] William Swenson, David Sloan Wilson, and Roberta Elias. Artificial ecosystem selection. *Proceedings of the National Academy of Sciences*, 97:9110–9114, 2000.

[9] W. Swenson, J. Arendt, and D.S. Wilson. Artificial selection of microbial ecosystems for 3-chloroaniline biodegradation. *Environ Microbiol*, 2(5):564–71, October 2000.

[10] Hywel T. P. Williams and Timothy M. Lenton. Artificial selection of simulated microbial ecosystems. *Proceedings of the National Academy of Sciences*, 104(21):8918–8923, May 2007. 00036.

[11] Kevin Panke-Buisse, Angela C Poole, Julia K Goodrich, Ruth E Ley, and Jenny Kao-Kniffin. Selection on soil microbiomes reveals reproducible impacts on plant function. *The ISME journal*, 9(4):980, 2015.

[12] Ulrich G Mueller, Thomas Juenger, Melissa Kardish, Alexis Carlson, Kathleen Burns, Chad Smith, and David De Marais. Artificial microbiome-selection to engineer microbiomes that confer salt-tolerance to plants. *bioRxiv*, page 081521, 2016.

[13] Charles J Goodnight. The influence of environmental variation on group and individual selection in a cress. *Evolution*, 39(3):545–558, 1985.

[14] Mitch D Day, Daniel Beck, and James A Foster. Microbial communities as experimental units. *Bioscience*, 61(5):398–406, 2011.

[15] U. G. Mueller and J. L. Sachs. Engineering Microbiomes to Improve Plant and Animal Health. *Trends in Microbiology*, 23(10):606–617, October 2015.

[16] Haoran Zhang, Brian Pereira, Zhengjun Li, and Gregory Stephanopoulos. Engineering escherichia coli coculture systems for the production of biochemical products. *Proceedings of the National Academy of Sciences*, page 201506781, 2015.

[17] Burton Simon, Jeffrey A Fletcher, and Michael Doebeli. Hamilton's rule in multi-level selection models. *Journal of theoretical biology*, 299:55–63, 2012.

[18] James A Damore and Jeff Gore. Understanding microbial cooperation. *Journal of theoretical biology*, 299:31–41, 2012.

[19] Babak Momeni, Li Xie, and Wenying Shou. Lotka-volterra pairwise modeling fails to capture diverse pairwise microbial interactions. *Elife*, 6, 2017.

[20] Jeremy J. Minty, Marc E. Singer, Scott A. Scholz, Chang-Hoon Bae, Jung-Ho Ahn, Clifton E. Foster, James C. Liao, and Xiaoxia Nina Lin. Design and characterization of synthetic fungal-bacterial consortia for direct production of isobutanol from cellulosic biomass. *Proceedings of the National Academy of Sciences*, 110(36):14592–14597, September 2013. 00024 PMID: 23959872.

[21] Kang Zhou, Kangjian Qiao, Steven Edgar, and Gregory Stephanopoulos. Distributing a metabolic pathway among a microbial consortium enhances production of natural products. *Nature biotechnology*, 2015.

[22] Hyun-Dong Shin, Shara McClendon, Trinh Vo, and Rachel R. Chen. Escherichia coli Binary Culture Engineered for Direct Fermentation of Hemicellulose to a Biofuel. *Applied and Environmental Microbiology*, 76(24):8150–8159, December 2010. 00000.

[23] Wenying Shou, Sri Ram, and Jose M. G. Vilar. Synthetic cooperation in engineered yeast populations. *Proceedings of the National Academy of Sciences of the United States of America*, 104(6):1877–1882, February 2007. 00137.

[24] Babak Momeni, Kristen A Brileya, Matthew W Fields, and Wenying Shou. Strong inter-population cooperation leads to partner intermixing in microbial communities. *eLife*, 2, January 2013.

[25] T Mankad and HR Bungay. Model for microbial growth with more than one limiting nutrient. *Journal of biotechnology*, 7(2):161–166, 1988.

[26] Sattar Taheri-Araghi, Serena Bradde, John T. Sauls, Norbert S. Hill, Petra Anne Levin, Johan Paulsson, Massimo Vergassola, and Suckjoon Jun. Cell-Size Control and Homeostasis in Bacteria. *Current Biology*, 25(3):385–391, February 2015.

[27] Richard E Lenski and Michael Travisano. Dynamics of adaptation and diversification: a 10,000-generation experiment with bacterial populations. *Proceedings of the National Academy of Sciences*, 91(15):6808–6814, 1994.

[28] Adam James Waite and Wenying Shou. Adaptation to a new environment allows cooperators to purge cheaters stochastically. *Proceedings of the National Academy of Sciences*, 109(47):19079–19086, 2012.

[29] Paul B Rainey and Katrina Rainey. Evolution of cooperation and conflict in experimental bacterial populations. *Nature*, 425(6953):72, 2003.

[30] Rafael U Ibarra, Jeremy S Edwards, and Bernhard O Palsson. Escherichia coli k-12 undergoes adaptive evolution to achieve in silico predicted optimal growth. *Nature*, 420(6912):186, 2002.

[31] Rafael Sanjuán, Andrés Moya, and Santiago F Elena. The distribution of fitness effects caused by single-nucleotide substitutions in an rna virus. *Proceedings of the National Academy of Sciences of the United States of America*, 101(22):8396–8401, 2004.

[32] Karen S Sarkisyan, Dmitry A Bolotin, Margarita V Meer, Dinara R Usmanova, Alexander S Mishin, George V Sharonov, Dmitry N Ivankov, Nina G Bozhanova, Mikhail S Baranov, Onuralp Soylemez, et al. Local fitness landscape of the green fluorescent protein. *Nature*, 533(7603):397–401, 2016.

[33] Dominika M Wloch, Krzysztof Szafraniec, Rhona H Borts, and Ryszard Korona. Direct estimate of the mutation rate and the distribution of fitness effects in the yeast saccharomyces cerevisiae. *Genetics*, 159(2):441–452, 2001.

[34] Celia Payen, Anna B Sunshine, Giang T Ong, Jamie L Pogachar, Wei Zhao, and Maitreya J Dunham. High-throughput identification of adaptive mutations in experimentally evolved yeast populations. *PLoS genetics*, 12(10):e1006339, 2016.

[35] Samuel Frederick Mock Hart, David Skelding, Adam J Waite, Justin Burton, Li Xie, and Wenying Shou. Microscopy quantification of microbial birth and death dynamics. *bioRxiv*, page 324269, 2018.

[36] Kristina L Hillesland and David A Stahl. Rapid evolution of stability and productivity at the origin of a microbial mutualism. *Proceedings of the National Academy of Sciences*, 107(5):2124–2129, 2010.

[37] Herwig Bachmann, Martin Fischlechner, Iraes Rabbers, Nakul Barfa, Filipe Branco dos Santos, Douwe Molenaar, and Bas Teusink. Availability of public goods shapes the evolution of competing metabolic strategies. *Proceedings of the National Academy of Sciences of the United States of America*, 110(35):14302–14307, August 2013.

[38] W. D. Hamilton. The genetical evolution of social behaviour I and II. *Journal of Theoretical Biology*, 7(1):1–52, July 1964.

[39] John Maynard Smith. Group Selection and Kin Selection. *Nature*, 201(4924):1145–1147, March 1964.

[40] Sewall Wright. Tempo and Mode in Evolution: A Critical Review. *Ecology*, 26(4):415–419, 1945.

[41] George R. Price. Selection and Covariance. *Nature*, 227(5257):520–521, August 1970. 01240.

[42] Michael J. Wade. A Critical Review of the Models of Group Selection. *The Quarterly Review of Biology*, 53(2):101–114, June 1978. ArticleType: research-article / Full publication date: Jun., 1978 / Copyright © 1978 The University of Chicago Press.

[43] William M Muir. Group selection for adaptation to multiple-hen cages: selection program and direct responses. *Poultry Science*, 75(4):447–458, 1996.

[44] David C. Queller and Joan E. Strassmann. Kin Selection and Social Insects. *BioScience*, 48(3):165–175, March 1998.

[45] Michael J Wade. An experimental study of kin selection. *Evolution*, pages 844–855, 1980.

[46] Arne Traulsen and Martin A. Nowak. Evolution of cooperation by multilevel selection. *Proceedings of the National Academy of Sciences*, 103(29):10952–10955, July 2006.

[47] L. Lehmann, L. Keller, S. West, and D. Roze. Group selection and kin selection: Two concepts but one process. *Proc Natl Acad Sci USA*, 104(16):6736–6739, April 2007.

[48] Benjamin Kerr. Theoretical and experimental approaches to the evolution of altruism and the levels of selection. *Experimental Evolution: Concepts, Methods, and Applications of Selection Experiments*, pages 585–630, 2009. 00006.

[49] Herwig Bachmann, Frank J Bruggeman, Douwe Molenaar, Filipe Branco dos Santos, and Bas Teusink. Public goods and metabolic strategies. *Current Opinion in Microbiology*, 31:109–115, June 2016. 00000.

[50] Katrin Hammerschmidt, Caroline J. Rose, Benjamin Kerr, and Paul B. Rainey. Life cycles, fitness decoupling and the evolution of multicellularity. *Nature*, 515(7525):75–79, November 2014.

[51] Martin A. Nowak. Five Rules for the Evolution of Cooperation. *Science*, 314(5805):1560–1563, December 2006.

[52] C. J. Goodnight and L. Stevens. Experimental studies of group selection: what do they tell us about group selection in nature? *The American Naturalist*, 150 Suppl 1:S59–79, July 1997.

[53] D. S. Wilson. A theory of group selection. *Proceedings of the National Academy of Sciences*, 72(1):143–146, January 1975.

[54] Michael E Gilpin. *Group selection in predator-prey communities*, volume 9. Princeton University Press, 1975.

[55] J. Maynard Smith. Group Selection. *The Quarterly Review of Biology*, 51(2):277–283, June 1976.

[56] Michael Doebeli, Yaroslav Ispolatov, and Burt Simon. Towards a mechanistic foundation of evolutionary theory. *eLife*, 6:e23804, February 2017.

[57] L. Chao and B.R. Levin. Structured habitats and the evolution of anticompetitor toxins in bacteria. *Proc Natl Acad Sci U S A*, 78(10):6324–8, October 1981.

[58] John S Chuang, Olivier Rivoire, and Stanislas Leibler. Simpson's paradox in a synthetic microbial system. *Science (New York, N.Y.)*, 323(5911):272–275, January 2009.

[59] George R Price. Extension of covariance selection mathematics. *Annals of human genetics*, 35(4):485–490, 1972.

[60] Li Xie and Wenying Shou. Community function landscape and steady state species composition shape the eco-evolutionary dynamics of arti1cial community selection. *bioRxiv*, page 264697, 2018.

[61] John L Spudich and Daniel E Koshland Jr. Non-genetic individuality: chance in the single cell. *Nature*, 262(5568):467, 1976.

[62] Stephen T Chisholm, Gitta Coaker, Brad Day, and Brian J Staskawicz. Host-microbe interactions: shaping the evolution of the plant immune response. *Cell*, 124(4):803–814, 2006.

[63] Ruth E Ley, Micah Hamady, Catherine Lozupone, Peter J Turnbaugh, Rob Roy Ramey, J Stephen Bircher, Michael L Schlegel, Tammy A Tucker, Mark D Schrenzel, Rob Knight, et al. Evolution of mammals and their gut microbes. *Science*, 320(5883):1647–1651, 2008.

[64] Kevin R Foster, Jonas Schluter, Katharine Z Coyte, and Seth Rakoff-Nahoum. The evolution of the host microbiome as an ecosystem on a leash. *Nature*, 548(7665):43, 2017.

[65] Luc De Vuyst, Raf Callewaert, and Kurt Crabbé. Primary metabolite kinetics of bacteriocin biosynthesis by Lactobacillus amylovorus and evidence for stimulation of bacteriocin production under unfavourable growth conditions. *Microbiology*, 142(4):817–827, 1996.

[66] Melanie JI Müller, Beverly I Neugeboren, David R Nelson, and Andrew W Murray. Genetic drift opposes mutualism during spatial population expansion. *Proceedings of the National Academy of Sciences*, 111(3):1037–1042, 2014.

[67] Thomas Egli. *Nutrition, microbial*. Oxford: Elsevier Academic Press, 2009.

[68] Kai Zhuang, Goutham N Vemuri, and Radhakrishnan Mahadevan. Economics of membrane occupancy and respiro-fermentation. *Molecular systems biology*, 7(1):500, 2011.

[69] Joan B Peris, Paulina Davis, José M Cuevas, Miguel R Nebot, and Rafael Sanjuán. Distribution of fitness effects caused by single-nucleotide substitutions in bacteriophage f1. *Genetics*, 185(2):603–609, 2010.

[70] Adrian WR Serohijos and Eugene I Shakhnovich. Merging molecular mechanism and evolution: theory and computation at the interface of biophysics and evolutionary population genetics. *Current opinion in structural biology*, 26:84–91, 2014.

[71] Adam Eyre-Walker and Peter D Keightley. The distribution of fitness effects of new mutations. *Nature reviews. Genetics*, 8(8):610, 2007.

[72] Michael A Stiffler, Doeke R Hekstra, and Rama Ranganathan. Evolvability as a function of purifying selection in tem-1 β-lactamase. *Cell*, 160(5):882–892, 2015.

[73] John W Drake. A constant rate of spontaneous mutation in dna-based microbes. *Proceedings of the National Academy of Sciences*, 88(16):7160–7164, 1991.

[74] Gregory I. Lang and Andrew W. Murray. Estimating the Per-Base-Pair Mutation Rate in the Yeast Saccharomyces cerevisiae. *Genetics*, 178(1):67–82, January 2008.

[75] Sasha F Levy, Jamie R Blundell, Sandeep Venkataram, Dmitri A Petrov, Daniel S Fisher, and Gavin Sherlock. Quantitative evolutionary dynamics using high-resolution lineage tracking. *Nature*, 519(7542):181, 2015.

[76] Clifford Zeyl and J Arjan GM DeVisser. Estimates of the rate and distribution of fitness effects of spontaneous mutation in saccharomyces cerevisiae. *Genetics*, 157(1):53–61, 2001.

[77] Jeffrey E Barrick, Dong Su Yu, Sung Ho Yoon, Haeyoung Jeong, Tae Kwang Oh, Dominique Schneider, Richard E Lenski, and Jihyun F Kim. Genome evolution and adaptation in a long-term experiment with escherichia coli. *Nature*, 461(7268):1243, 2009.

[78] Toon Swings, Bram Van den Bergh, Sander Wuyts, Eline Oeyen, Karin Voordeckers, Kevin J Verstrepen, Maarten Fauvart, Natalie Verstraeten, and Jan Michiels. Adaptive tuning of mutation rates allows fast response to lethal stress in escherichia coli. *eLife*, 6(22939), 2017.

[79] Lília Perfeito, Lisete Fernandes, Catarina Mota, and Isabel Gordo. Adaptive mutations in bacteria: high rate and small effects. *Science*, 317(5839):813–815, 2007.

[80] John H Gillespie. Molecular evolution over the mutational landscape. *Evolution*, 38(5):1116–1129, 1984.

[81] H Allen Orr. The distribution of fitness effects among beneficial mutations. *Genetics*, 163(4):1519–1526, 2003.

[82] Marianne Imhof and Christian Schlötterer. Fitness effects of advantageous mutations in evolving escherichia coli populations. *Proceedings of the National Academy of Sciences*, 98(3):1113–1117, 2001.

[83] Rees Kassen and Thomas Bataillon. Distribution of fitness effects among beneficial mutations before selection in experimental populations of bacteria. *Nature genetics*, 38(4):484, 2006.

[84] Darin R Rokyta, Paul Joyce, S Brian Caudle, and Holly A Wichman. An empirical test of the mutational landscape model of adaptation using a single-stranded dna virus. *Nature genetics*, 37(4):441, 2005.

[85] Darin R Rokyta, Craig J Beisel, Paul Joyce, Martin T Ferris, Christina L Burch, and Holly A Wichman. Beneficial fitness effects are not exponential for two viruses. *Journal of molecular evolution*, 67(4):368, 2008.

[86] Michael J Wiser, Noah Ribeck, and Richard E Lenski. Long-term dynamics of adaptation in asexual populations. *Science*, 342(6164):1364–1367, 2013.

[87] Lukasz Jasnos and Ryszard Korona. Epistatic buffering of fitness loss in yeast double deletion strains. *Nature genetics*, 39(4):550, 2007.

[88] Rafael Sanjuán, Andrés Moya, and Santiago F Elena. The contribution of epistasis to the architecture of fitness in an rna virus. *Proceedings of the National Academy of Sciences of the United States of America*, 101(43):15376–15379, 2004.

[89] Aisha I Khan, Duy M Dinh, Dominique Schneider, Richard E Lenski, and Tim F Cooper. Negative epistasis between beneficial mutations in an evolving bacterial population. *Science*, 332(6034):1193–1196, 2011.

[90] Santiago F Elena and Richard E Lenski. Test of synergistic interactions among deleterious mutations in bacteria. *Nature*, 390(6658):395, 1997.

[91] Carlos L Araya, Douglas M Fowler, Wentao Chen, Ike Muniez, Jeffery W Kelly, and Stanley Fields. A fundamental protein property, thermodynamic stability, revealed solely from large-scale measurements of protein function. *Proceedings of the National Academy of Sciences*, 109(42):16858–16863, 2012.

[92] Hsin-Hung Chou, Hsuan-Chao Chiu, Nigel F Delaney, Daniel Segrè, and Christopher J Marx. Diminishing returns epistasis among beneficial mutations decelerates adaptation. *Science*, 332(6034):1190–1192, 2011.

[93] Sergey Kryazhimskiy, Daniel P Rice, Elizabeth R Jerison, and Michael M Desai. Global epistasis makes adaptation predictable despite sequence-level stochasticity. *Science*, 344(6191):1519–1522, 2014.

[94] G. W. Luli and W. R. Strohl. Comparison of growth, acetate production, and acetate inhibition of Escherichia coli strains in batch and fed-batch fermentations. *Applied and Environmental Microbiology*, 56(4):1004–1011, April 1990.

[95] Wenying Shou. Acknowledging selection at sub-organismal levels resolves controversy on pro-cooperation mechanisms. *eLife*, page e10106, December 2015.

[96] R C Lewontin. The Units of Selection. *Annual Review of Ecology and Systematics*, 1(1):1–18, 1970.

[97] A. Crameri, E. A. Whitehorn, E. Tate, and W. P. Stemmer. Improved green fluorescent protein by molecular evolution using DNA shuffling. *Nature Biotechnology*, 14(3):315–319, March 1996.

[98] Manfred T. Reetz and José Daniel Carballeira. Iterative saturation mutagenesis (ISM) for rapid directed evolution of functional enzymes. *Nature Protocols*, 2(4):891–903, April 2007.

[99] Eric T. Boder, Katarina S. Midelfort, and K. Dane Wittrup. Directed evolution of antibody fragments with monovalent femtomolar antigen-binding affinity. *Proceedings of the National Academy of Sciences*, 97(20):10701–10705, September 2000.